



**HAL**  
open science

## Changes of physico-chemical properties of nano-biomaterials by digestion fluids affect the physiological properties of epithelial intestinal cells and barrier models

Giulia Antonello, Arianna Marucco, Elena Gazzano, Panagiotis Kainourgios, Costanza Ravagli, Ana Gonzalez-Paredes, Simone Sprio, Esperanza Padín-González, Mahmoud Soliman, David Beal, et al.

► **To cite this version:**

Giulia Antonello, Arianna Marucco, Elena Gazzano, Panagiotis Kainourgios, Costanza Ravagli, et al.. Changes of physico-chemical properties of nano-biomaterials by digestion fluids affect the physiological properties of epithelial intestinal cells and barrier models. *Particle and Fibre Toxicology*, 2022, 19 (1), pp.49. 10.1186/s12989-022-00491-w . hal-03841933

**HAL Id: hal-03841933**

**<https://hal.science/hal-03841933>**

Submitted on 7 Nov 2022

**HAL** is a multi-disciplinary open access archive for the deposit and dissemination of scientific research documents, whether they are published or not. The documents may come from teaching and research institutions in France or abroad, or from public or private research centers.

L'archive ouverte pluridisciplinaire **HAL**, est destinée au dépôt et à la diffusion de documents scientifiques de niveau recherche, publiés ou non, émanant des établissements d'enseignement et de recherche français ou étrangers, des laboratoires publics ou privés.

# Metadata of the article that will be visualized in OnlineFirst

---

ArticleTitle	Changes of physico-chemical properties of nano-biomaterials by digestion fluids affect the physiological properties of epithelial intestinal cells and barrier models	
--------------	---	--

---

Article Sub-Title		
-------------------	--	--

---

Article CopyRight	The Author(s) (This will be the copyright line in the final PDF)	
-------------------	---	--

---

Journal Name	Particle and Fibre Toxicology	
--------------	-------------------------------	--

---

Corresponding Author	FamilyName	<b>Fenoglio</b>
	Particle	
	Given Name	<b>Ivana</b>
	Suffix	
	Division	Department of Chemistry
	Organization	University of Turin
	Address	Via Pietro Giuria 7, 10125, Turin, Italy
	Phone	
	Fax	
	Email	ivana.fenoglio@unito.it
	URL	
	ORCID	

---

Corresponding Author	FamilyName	<b>Riganti</b>
	Particle	
	Given Name	<b>Chiara</b>
	Suffix	
	Division	Department of Oncology
	Organization	University of Turin
	Address	Via Santena 5 bis, 10126, Turin, Italy
	Phone	
	Fax	
	Email	chiara.riganti@unito.it
	URL	
	ORCID	

---

Author	FamilyName	<b>Antonello</b>
	Particle	
	Given Name	<b>Giulia</b>
	Suffix	
	Division	Department of Chemistry
	Organization	University of Turin
	Address	Via Pietro Giuria 7, 10125, Turin, Italy
	Division	Department of Public Health and Pediatrics
	Organization	University of Turin
	Address	Piazza Polonia, 94, 10126, Turin, Italy
	Division	Department of Oncology
	Organization	University of Turin
	Address	Via Santena 5 bis, 10126, Turin, Italy
	Phone	
	Fax	
	Email	
URL		

ORCID

---

Author	FamilyName	<b>Marucco</b>
	Particle	
	Given Name	<b>Arianna</b>
	Suffix	
	Division	Department of Life Sciences and Systems Biology
	Organization	University of Turin
	Address	Via Accademia Albertina 13, 10123, Turin, Italy
	Phone	
	Fax	
	Email	
	URL	
	ORCID	

---

Author	FamilyName	<b>Gazzano</b>
	Particle	
	Given Name	<b>Elena</b>
	Suffix	
	Division	Department of Life Sciences and Systems Biology
	Organization	University of Turin
	Address	Via Accademia Albertina 13, 10123, Turin, Italy
	Phone	
	Fax	
	Email	
	URL	
	ORCID	

---

Author	FamilyName	<b>Kainourgios</b>
	Particle	
	Given Name	<b>Panagiotis</b>
	Suffix	
	Division	Research Unit of Advanced, Composite, Nano-Materials and Nanotechnology, School of Chemical Engineering
	Organization	National Technical University of Athens
	Address	9 Heroon Polytechniou St., 15780, Zographos, Athens, Greece
	Phone	
	Fax	
	Email	
	URL	
	ORCID	

---

Author	FamilyName	<b>Ravagli</b>
	Particle	
	Given Name	<b>Costanza</b>
	Suffix	
	Division	
	Organization	Colorobbia Consulting Srl, Headwork
	Address	Via Pietramarina, 53, 50059, Sovigliana, Vinci, FI, Italy
	Phone	
	Fax	
	Email	
	URL	
	ORCID	

---

Author	FamilyName	<b>Gonzalez-Paredes</b>
	Particle	
	Given Name	<b>Ana</b>
	Suffix	

Division  
Organization Nanovector Srl, Headwork  
Address Via Livorno 60, 10144, Turin, Italy  
Phone  
Fax  
Email  
URL  
ORCID

---

Author                      FamilyName                      **Sprio**  
Particle  
Given Name                      **Simone**  
Suffix  
Division  
Organization                      National Research Council, Institute of Science and Technology for Ceramics  
ISTEC-CNR  
Address                      Via Granarolo 64, 48018, Faenza, RA, Italy  
Phone  
Fax  
Email  
URL  
ORCID

---

Author                      FamilyName                      **Padín-González**  
Particle  
Given Name                      **Esperanza**  
Suffix  
Division                      Department of Chemistry  
Organization                      Royal College of Surgeons in Ireland (RCSI)  
Address                      123 St Stephen Green, Dublin 2, Ireland  
Phone  
Fax  
Email  
URL  
ORCID

---

Author                      FamilyName                      **Soliman**  
Particle  
Given Name                      **Mahmoud G.**  
Suffix  
Division                      Department of Chemistry  
Organization                      Royal College of Surgeons in Ireland (RCSI)  
Address                      123 St Stephen Green, Dublin 2, Ireland  
Phone  
Fax  
Email  
URL  
ORCID

---

Author                      FamilyName                      **Beal**  
Particle  
Given Name                      **David**  
Suffix  
Division                      CEA, CNRS, IRIG, SyMMES-CIBEST  
Organization                      Université Grenoble Alpes  
Address                      38000, Grenoble, France  
Phone  
Fax

Email  
URL  
ORCID

---

Author	FamilyName	<b>Barbero</b>
	Particle	
	Given Name	<b>Francesco</b>
	Suffix	
	Division	Department of Chemistry
	Organization	University of Turin
	Address	Via Pietro Giuria 7, 10125, Turin, Italy
	Phone	
	Fax	
	Email	
	URL	
	ORCID	

---

Author	FamilyName	<b>Gasco</b>
	Particle	
	Given Name	<b>Paolo</b>
	Suffix	
	Division	
	Organization	Nanovector Srl, Headwork
	Address	Via Livorno 60, 10144, Turin, Italy
	Phone	
	Fax	
	Email	
	URL	
	ORCID	

---

Author	FamilyName	<b>Baldi</b>
	Particle	
	Given Name	<b>Giovanni</b>
	Suffix	
	Division	
	Organization	Colorobbia Consulting Srl, Headwork
	Address	Via Pietramarina, 53, 50059, Sovigliana, Vinci, FI, Italy
	Phone	
	Fax	
	Email	
	URL	
	ORCID	

---

Author	FamilyName	<b>Carriere</b>
	Particle	
	Given Name	<b>Marie</b>
	Suffix	
	Division	CEA, CNRS, IRIG, SyMMES-CIBEST
	Organization	Université Grenoble Alpes
	Address	38000, Grenoble, France
	Phone	
	Fax	
	Email	
	URL	
	ORCID	

---

Author	FamilyName	<b>Monopoli</b>
	Particle	

Given Name **Marco P.**  
Suffix  
Division Department of Chemistry  
Organization Royal College of Surgeons in Ireland (RCSI)  
Address 123 St Stephen Green, Dublin 2, Ireland  
Phone  
Fax  
Email  
URL  
ORCID

---

Author FamilyName **Charitidis**  
Particle  
Given Name **Costas A.**  
Suffix  
Division Research Unit of Advanced, Composite, Nano-Materials and  
Nanotechnology, School of Chemical Engineering  
Organization National Technical University of Athens  
Address 9 Heroon Polytechniou St., 15780, Zographos, Athens, Greece  
Phone  
Fax  
Email  
URL  
ORCID

---

Author FamilyName **Bergamaschi**  
Particle  
Given Name **Enrico**  
Suffix  
Division Department of Public Health and Pediatrics  
Organization University of Turin  
Address Piazza Polonia, 94, 10126, Turin, Italy  
Phone  
Fax  
Email  
URL  
ORCID

---

Schedule Received 9 Feb 2022  
Revised  
Accepted 29 Jun 2022

---

Abstract *Background:*  
The widespread use of nano-biomaterials (NBMs) has increased the chance of human exposure. Although ingestion is one of the major routes of exposure to NBMs, it is not thoroughly studied to date. NBMs are expected to be dramatically modified following the transit into the oral-gastric-intestinal (OGI) tract. How these transformations affect their interaction with intestinal cells is still poorly understood. NBMs of different chemical nature—lipid-surfactant nanoparticles (LSNPs), carbon nanoparticles (CNPs), surface modified Fe<sub>3</sub>O<sub>4</sub> nanoparticles (FNPs) and hydroxyapatite nanoparticles (HNPs)—were treated in a simulated human digestive system (SHDS) and then characterised. The biological effects of SHDS-treated and untreated NBMs were evaluated on primary (HCoEpiC) and immortalised (Caco-2, HCT116) epithelial intestinal cells and on an intestinal barrier model.  
*Results:*  
The application of the in vitro SHDS modified the biocompatibility of NBMs on gastrointestinal cells. The differences between SHDS-treated and untreated NBMs could be attributed to the irreversible modification of the NBMs in the SHDS. Aggregation was detected for all NBMs regardless of their chemical nature, while pH- or enzyme-mediated partial degradation was detected for hydroxyapatite or polymer-coated iron oxide nanoparticles and lipid nanoparticles, respectively. The formation of a bio-corona, which contains proteases, was also demonstrated on all the analysed NBMs. In viability assays, undifferentiated primary cells were more sensitive than immortalised cells to digested NBMs, but neither pristine nor treated NBMs affected the intestinal barrier viability and permeability. SHDS-treated NBMs

up-regulated the tight junction genes (claudin 3 and 5, occludin, zonula occludens 1) in intestinal barrier, with different patterns between each NBM, and increase the expression of both pro- and anti-inflammatory cytokines (IL-1 $\beta$ , TNF- $\alpha$ , IL-22, IL-10). Notably, none of these NBMs showed any significant genotoxic effect.

*Conclusions:*

Overall, the results add a piece of evidence on the importance of applying validated in vitro SHDS models for the assessment of NBM intestinal toxicity/biocompatibility. We propose the association of chemical and microscopic characterization, SHDS and in vitro tests on both immortalised and primary cells as a robust screening pipeline useful to monitor the changes in the physico-chemical properties of ingested NBMs and their effects on intestinal cells.

---

Keywords (separated by '-') Nano-biomaterials - In vitro simulated digestion - Biotransformation - Toxicity - Caco-2 - HCT116 - HCoEpiC - Gastro-intestinal barrier - Permeability - Inflammation

---

Footnote Information Ivana Fenoglio and Chiara Riganti contributed equally to this workThe online version contains supplementary material available at <https://doi.org/10.1186/s12989-022-00491-w>.

---

RESEARCH

Open Access



# Changes of physico-chemical properties of nano-biomaterials by digestion fluids affect the physiological properties of epithelial intestinal cells and barrier models

Giulia Antonello<sup>1,2,3</sup>, Arianna Marucco<sup>4</sup>, Elena Gazzano<sup>4</sup>, Panagiotis Kainourgios<sup>5</sup>, Costanza Ravagli<sup>6</sup>, Ana Gonzalez-Paredes<sup>7</sup>, Simone Sprio<sup>8</sup>, Esperanza Padín-González<sup>9</sup>, Mahmoud G. Soliman<sup>9</sup>, David Beal<sup>10</sup>, Francesco Barbero<sup>1</sup>, Paolo Gasco<sup>7</sup>, Giovanni Baldi<sup>6</sup>, Marie Carriere<sup>10</sup>, Marco P. Monopoli<sup>9</sup>, Costas A. Charitidis<sup>5</sup>, Enrico Bergamaschi<sup>2</sup>, Ivana Fenoglio<sup>1\*†</sup> and Chiara Riganti<sup>3\*†</sup>

## Abstract

**Background:** The widespread use of nano-biomaterials (NBMs) has increased the chance of human exposure. Although ingestion is one of the major routes of exposure to NBMs, it is not thoroughly studied to date. NBMs are expected to be dramatically modified following the transit into the oral-gastric-intestinal (OGI) tract. How these transformations affect their interaction with intestinal cells is still poorly understood. NBMs of different chemical nature—lipid-surfactant nanoparticles (LSNPs), carbon nanoparticles (CNPs), surface modified Fe<sub>3</sub>O<sub>4</sub> nanoparticles (FNPs) and hydroxyapatite nanoparticles (HNPs)—were treated in a simulated human digestive system (SHDS) and then characterised. The biological effects of SHDS-treated and untreated NBMs were evaluated on primary (HCoEpiC) and immortalised (Caco-2, HCT116) epithelial intestinal cells and on an intestinal barrier model.

**Results:** The application of the in vitro SHDS modified the biocompatibility of NBMs on gastrointestinal cells. The differences between SHDS-treated and untreated NBMs could be attributed to the irreversible modification of the NBMs in the SHDS. Aggregation was detected for all NBMs regardless of their chemical nature, while pH- or enzyme-mediated partial degradation was detected for hydroxyapatite or polymer-coated iron oxide nanoparticles and lipid nanoparticles, respectively. The formation of a bio-corona, which contains proteases, was also demonstrated on all the analysed NBMs. In viability assays, undifferentiated primary cells were more sensitive than immortalised cells to digested NBMs, but neither pristine nor treated NBMs affected the intestinal barrier viability and permeability. SHDS-treated NBMs up-regulated the tight junction genes (claudin 3 and 5, occludin, zonula occludens 1) in intestinal barrier, with different patterns between each NBM, and increase the expression of both pro- and anti-inflammatory cytokines (IL-1 $\beta$ , TNF- $\alpha$ , IL-22, IL-10). Notably, none of these NBMs showed any significant genotoxic effect.

AQ1

<sup>†</sup>Ivana Fenoglio and Chiara Riganti contributed equally to this work

\*Correspondence: ivana.fenoglio@unito.it; chiara.riganti@unito.it

<sup>1</sup> Department of Chemistry, University of Turin, Via Pietro Giuria 7, 10125 Turin, Italy

<sup>3</sup> Department of Oncology, University of Turin, Via Santena 5 bis, 10126 Turin, Italy

Full list of author information is available at the end of the article



© The Author(s) 2022. **Open Access** This article is licensed under a Creative Commons Attribution 4.0 International License, which permits use, sharing, adaptation, distribution and reproduction in any medium or format, as long as you give appropriate credit to the original author(s) and the source, provide a link to the Creative Commons licence, and indicate if changes were made. The images or other third party material in this article are included in the article's Creative Commons licence, unless indicated otherwise in a credit line to the material. If material is not included in the article's Creative Commons licence and your intended use is not permitted by statutory regulation or exceeds the permitted use, you will need to obtain permission directly from the copyright holder. To view a copy of this licence, visit <http://creativecommons.org/licenses/by/4.0/>. The Creative Commons Public Domain Dedication waiver (<http://creativecommons.org/publicdomain/zero/1.0/>) applies to the data made available in this article, unless otherwise stated in a credit line to the data.



Journal : **BMCTwo 12989**

Dispatch : **7-7-2022**

Pages : **28**

Article No : **491**

LE

TYPESET

MS Code :

CP

DISK



**Conclusions:** Overall, the results add a piece of evidence on the importance of applying validated in vitro SHDS models for the assessment of NBM intestinal toxicity/biocompatibility. We propose the association of chemical and microscopic characterization, SHDS and in vitro tests on both immortalised and primary cells as a robust screening pipeline useful to monitor the changes in the physico-chemical properties of ingested NBMs and their effects on intestinal cells.

**Keywords:** Nano-biomaterials, In vitro simulated digestion, Biotransformation, Toxicity, Caco-2, HCT116, HCoEpiC, Gastro-intestinal barrier, Permeability, Inflammation

## Background

In the last few years, nano-biomaterials (NBMs) have been widely used for manufacturing innovative food packaging [1, 2] nutraceuticals [3], cosmetics [4, 5], as well as in dentistry [6], precision medicine [7–9] and agriculture [10, 11], increasing the likelihood of human exposure through ingestion and transit through the gastro-intestinal (GI) tract [12].

A growing number of studies suggested a possible interference of ingested NBMs with the gut microenvironment [13]. The human digestive apparatus is composed of many sections with different structures and functions. The most complex part is the intestinal tract. In particular, the small intestine mediates the absorption of nutrients through transcellular processes or paracellular diffusion. The latter is limited by the presence of tight junction (TJs) complexes, formed by zonula occludens-1, occludin and claudin proteins [14]. In physiological conditions, TJs prevent water and electrolyte leakage and avoid lumen infections. However, some conditions, such as inflammatory bowel disease [15, 16], can alter the structure of TJs, increasing the intestinal barrier permeability. Two studies report that nanometric SiO<sub>2</sub> or TiO<sub>2</sub> can induce similar effects [17, 18].

While a substantial amount of knowledge has been accumulated for the inhalation route, only recently the fate of the ingested NBMs has gained interest in the nanotoxicology community [19]. The poor awareness of ingestion's relevance as exposure route to NBMs, the non-suitability of the available models, and the lack of consensus on the most suitable in vitro models reproducing the complexity of the Oral-Gastro-Intestinal (OGI) tract are the main reasons for this delay.

In the last few years, some models to mimic the intestinal barrier in vitro and study the toxicity of NBM have been proposed, as co-cultures of different intestinal cell types. Co-culture monolayers, composed by enterocyte-like cells with TJs and brush border (Caco-2), and goblet cells secreting mucus (HT29-MTX), have been used to investigate the toxicity of NBMs such as TiO<sub>2</sub> nanoparticles [20–23] and multi walled carbon nanotubes [24]. The effect of halloysite clay nanotube on intestinal barrier [25] has been also studied on Caco-2/HT29-MTX

co-culture plus Raji B cells (that promote Caco-2 differentiation into M cells, characterised by the typical digestive function of enterocytes). The results have indicated the absence of cytotoxicity despite the high production of pro-inflammatory cytokines and the increase in cell growth and proliferation [26].

Recently, newly intestinal mucosa 3D models have been developed culturing Caco-2 cells on a layer of macrophages and dendritic cells embedded in collagen scaffolds. Indeed, these immune cells are both present in the intestinal lamina propria and react to inflammatory stimuli, by producing pro-inflammatory cytokines (e.g. interleukin (IL)-6, tumour necrosis factor (TNF)- $\alpha$ ) and anti-inflammatory mediator (e.g. IL-10) [27, 28], as a possible compensation mechanism. Interestingly, some of these mediators such as IL-6 and TNF- $\alpha$  are involved in the pathogenesis of inflammatory bowel disease, promoting gut damage and loss of intestinal barrier integrity, while IL-10 reduces the inflammation typically associated with this pathology [29]. Some NBMs have been shown to induce intestinal cells to assume the phenotype of inflammatory bowel disease. For instance, the model proposed by Susewind and co-workers to assess the safety of TiO<sub>2</sub>, Ag and Au nanoparticles [30] is characterised by the loss of barrier function and the increased production of inflammatory cytokines that regress after the treatment with anti-inflammatory drugs [31], well recapitulating the situation occurring in vivo.

Furthermore, some authors proposed *ex-vivo* systems derived from murine, porcine, or human bowel to study the intestinal permeability after the exposure to nanoparticles [32, 33].

Although these models are closer to the intestinal anatomy and physiology than conventional monocultures, the most used model for the evaluation of the exposure to NBMs is still the culture of Caco-2 cells on porous membrane inserts. In these conditions the cells rapidly differentiate into an intestinal barrier [34–37]. In addition the HCT116 model, another colon cancer cell line, is a widely accepted tool to evaluate the genotoxicity of NBMs [38–41].

Another important issue to be considered in in vitro intestinal models is the biological identity of the NBMs



122 that are in contact with cells, because ingested NBMs  
123 interact with different fluids characterised by specific  
124 pH, ionic strength, and composition. This interaction  
125 may dramatically modify NBMs' properties. For instance,  
126 the exposure may lead to dissolution [42], aggregation/  
127 agglomeration [43], and formation of bio-molecular  
128 corona [44] that may change over time. Monitoring such  
129 biotransformations is crucial to understand the NBMs  
130 biological fate in the gut environment and the impact on  
131 their toxicity [19, 45].

132 Recently, several in vitro digestion models have been  
133 proposed to investigate the digestion-driven modifica-  
134 tions of NBMs. Sequential incubations in simulated  
135 gastric and intestinal fluids have been used to study the  
136 bioactivity of starch nanocapsules [46] and zein-pectin  
137 nanoparticles [47]. A similar protocol, improved with  
138 longer incubation times and the addition of simulated  
139 saliva, has been set up to study the dissolution of Fe<sub>2</sub>O<sub>3</sub>  
140 nanoparticles [48], the agglomeration of TiO<sub>2</sub> nanoparti-  
141 cles and their interaction with proteins [49]. Several other  
142 models have been proposed, differing in fluid composi-  
143 tion or incubation times, such as the simulated digestion  
144 system reported in Sohal et al. [50] and slightly modified  
145 by Marucco et al. [39]. Most of these models have been  
146 used to describe the transformation occurring to NBMs  
147 during the digestive process. Nevertheless, few stud-  
148 ies have been published on the effects that such changes  
149 have on intestinal cells [51–54].

150 To fill this gap, in this study we adopted a simulated  
151 human digestion system (SHDS) consisting of sequen-  
152 tial incubations in simulated saliva fluid (SSF), simulated  
153 gastric fluid (SGF) and simulated intestinal fluid (SIF) to  
154 investigate the biotransformation of NBMs of different  
155 chemical nature. Samples representative of NBMs with  
156 potential applications in oral drug delivery or nutraceu-  
157 tical field have been selected, i.e. hydroxyapatite, carbon

158 nanoparticles, lipid-surfactant nanoparticles and surface  
159 modified magnetite nanoparticles [55–58]. The effects  
160 of SHDS-treated or untreated NBMs on viability, barrier  
161 integrity and intracellular inflammation were evaluated  
162 on primary and immortalised epithelial intestinal cells.

## 163 Results

### 164 Properties of the NBMs

165 In this study, we selected the following NBMs: three col-  
166 loidal formulations composed by elemental carbon nano-  
167 particles (CNPs), lipid-surfactant nanoparticles (LSNPs)  
168 and PLGA-PEG coated magnetite nanoparticles (FNPs),  
169 and one powder sample of hydroxyapatite nanoparticles  
170 (HNPs).

171 The main properties of the materials are summarized  
172 in Table 1.

173 The size distribution and the surface properties of  
174 the NBMs were investigated by Dynamic Light Scatter-  
175 ing (DLS) and Electrophoretic Light Scattering (ELS),  
176 respectively (Table 1 and Fig. 1A and B).

177 Because of the presence of particles/aggregates larger  
178 than the upper limit of detection of the DLS technique  
179 (5 μm), LSNPs and HNPs were also analysed by flow  
180 particle imaging analysis (FPIA) (size range 1–150 μm)  
181 (Fig. 1C and D).

182 Based on the low polydispersity index (PDI) values  
183 and on the small standard deviation (SD) of the size  
184 distribution (Table 1), CNPs and FNPs appeared sta-  
185 ble and monodisperse colloidal suspensions. CNPs  
186 and FNPs were mainly composed of nanometric parti-  
187 cles (< 100 nm), albeit particles/agglomerates or aggre-  
188 gates in the nanometric/sub-micrometric range were  
189 detected as well (Fig. 1A). According to DLS, LSNPs  
190 had a larger size than CNPs and FNPs, mainly in the  
191 sub-micrometric range (Fig. 1A). However, it might  
192 correspond to the presence of few sub-micrometric

**Table 1** Physico-chemical properties of samples

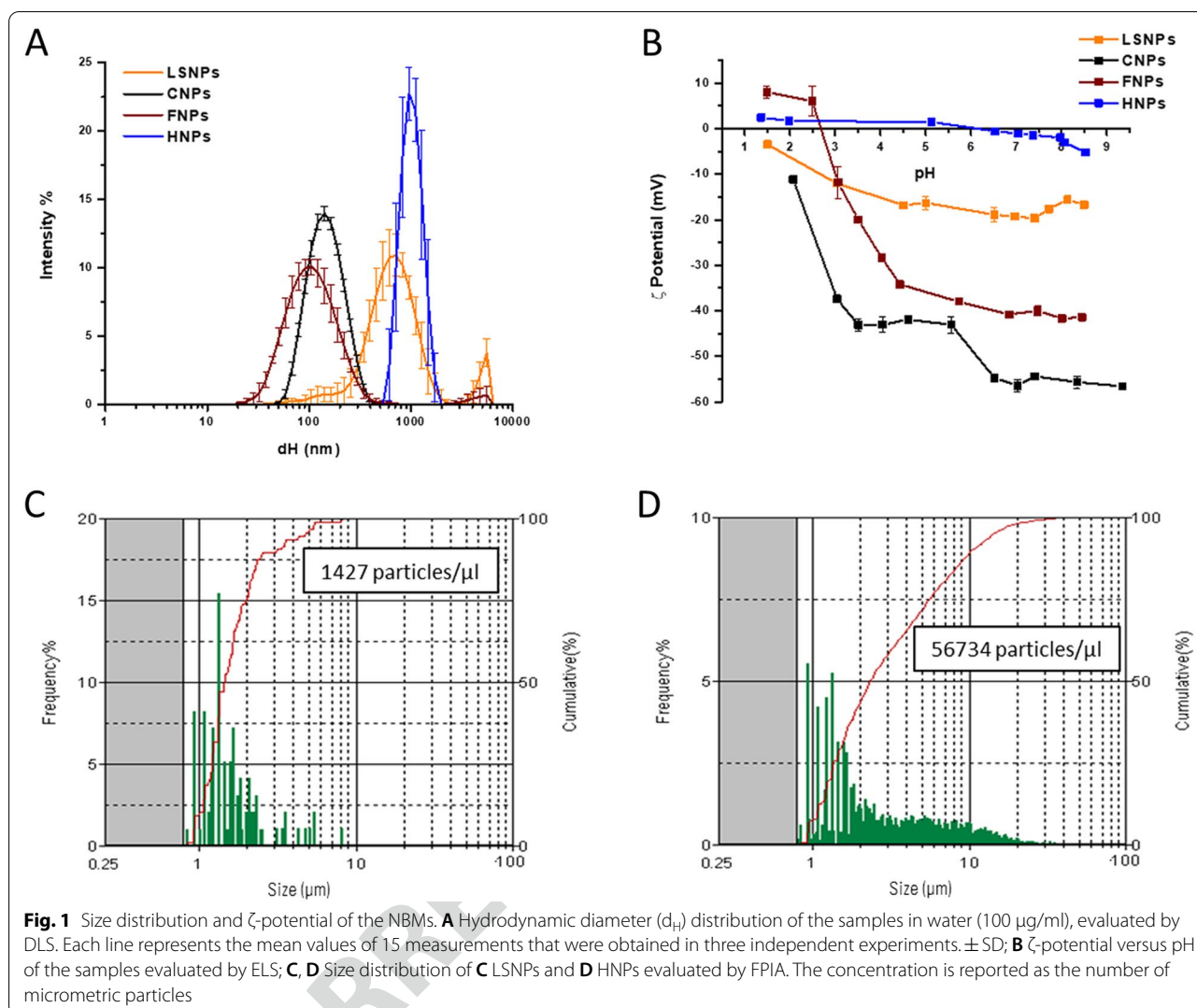
Samples	Appearance	Concentration (mg/ml)	Z-average hydrodynamic diameter (nm)*	ζ-potential (mV)**	Suspension pH**
LSNPs Lipid-surfactant nanoparticles	Colloidal suspension	12	135.0 ± 0.5 PDI 0.244	-16.3 ± 1.5	5.46
CNPs Carbon nanoparticles	Colloidal suspension	1.2	130.8 ± 1.0 PDI 0.170	-52.6 ± 1.0	4.60
FNPs PLGA-PEG coated Fe <sub>3</sub> O <sub>4</sub> nanoparticles	Colloidal suspension	2	83.2 ± 0.5 PDI 0.169	-40.8 ± 1.0	6.84
HNPs Hydroxyapatite nanoparticles	Powder	1	3126 ± 523 PDI 0.648	-2.0 ± 0.2	7.75

PDI is referred to Polydispersity Index

\* DLS measurement, samples diluted in water (100 μg/ml)

\*\* ELS and pH measurement, samples diluted in water (100 μg/ml)





193 particles, since DLS techniques overestimate the abun-  
 194 dant of particles with larger sizes. FPIA confirms the  
 195 presence of few particles with a diameter between 1  
 196 and 10  $\mu\text{m}$  (Fig. 1C). As far as HNPs are concerned,  
 197 particles were distributed in a wide range of sizes, from  
 198 400 nm to 20  $\mu\text{m}$  (Fig. 1D). In water HNPs formed  
 199 unstable suspensions, with clear sedimentation during  
 200 time. More details on the structure of the four NBMs  
 201 were provided by transmission electron microscope  
 202 (TEM) analysis (following section). As expected, LSNPs  
 203 and CNPs exhibited negative  $\zeta$ -potential values in the  
 204 whole pH range (Fig. 1B), suggesting the presence  
 205 of negatively charged surface groups. FNPs showed  
 206 positive  $\zeta$ -potential values only at very low pH values  
 207 (Fig. 1B), likely because of the contribution of the mag-  
 208 netite core. HNPs had  $\zeta$ -potential values close to 0 mV  
 209 at all pH (Fig. 1B) that well agree with the instability of  
 210 the suspensions.

**Effect of the simulated human digestive system (SHDS)  
 on the measured particles size**

The transformation of the NBMs was monitored in terms  
 of changes in size distribution, surface modifications, and  
 degradation or dissolution by enzymatic digestion.

The changes in size distribution of NBMs during the  
 SHDS treatment were firstly measured by integrating  
 DLS and FPIA data. In Fig. 2 the hydrodynamic distribu-  
 tion in the different compartments was compared with  
 those measured in water.

No changes of size distribution were found for LSNPs  
 and CNPs in SSF (Fig. 2A and B), while a shift of the dis-  
 tribution curve toward higher diameters was observed  
 for FNPs (Fig. 2C), suggesting agglomeration/aggrega-  
 tion. In the SGF a clear destabilization of the colloidal  
 suspensions was observed for all NBMs, as inferred by  
 the diameters shift towards high values and the increase  
 in the standard deviation among the measurements

(Fig. 2A–D). This was expected, because of the low pH and high ionic strength of the media. Because of the intrinsic instability of HNP suspension, the effect of the SGF was less evident (Fig. 2D). The suspensions remained highly unstable also in the SIF and the presence of large aggregates was optically visible in the final suspension (Additional file 1: Fig S1). The presence of micrometric particles/aggregates was evaluated by FPIA (Fig. 2E–H). Micrometric particles were detected in all cases, albeit in different amounts. LSNPs (Fig. 2E) exhibited a concentration of micrometric particles higher than the untreated material, while for HNPs (Fig. 2H) a decrease was observed.

The size distribution was also measured by incubating the NBMs directly in the intestinal fluid (Additional file 1: Fig S2). In this case, the suspension appeared more stable and less aggregated than after the SHDS, suggesting that the aggregation occurred in the SGF, and was irreversible for all NBMs.

TEM analysis of the SHDS-treated and untreated NBMs was also performed (Fig. 3).

Untreated LSNPs (Fig. 3A) were composed by quasi-spherical particles of different size, confirming the DLS analysis (Fig. 1A). SHDS-treated LSNPs (Fig. 3A') appeared of smaller dimensions, suggesting degradation, but organized in large aggregates surrounded by biological material deriving from the SHDS fluids.

Untreated CNPs (Fig. 3B) appeared spherical, well dispersed, and had a narrow size distribution around 120 nm, in agreement with the DLS data, whereas the SHDS-treated CNPs (Fig. 3B') resulted in an agglomerated and entangled state with associated biological material, similarly to LSNPs (Fig. 3A').

Untreated FNPs (Fig. 3C) appeared as small spherical iron oxide particles embedded inside the PLGA-PEG polymer matrix. After the SHDS (Fig. 3C') the polymer matrix was apparently removed, likely because of the biodegradable nature of the PLGA polymer [59]. Transparent spherical structures, which can be attributed to the polymeric residues still present after a partial biodegradation or to the biological matrix, were visible. Iron oxide particles appeared highly aggregated, because of the degradation of the polymeric matrix, in line with the results obtained by the DLS analyses (Fig. 2C). No significant alterations of the iron oxide particles morphology were observed.

Large particles of very different shapes such as rods, rectangles or spheres were observed for HNPs (Fig. 3D).

This shape/size diversity can justify the instability of the colloidal suspensions and the inconclusive results in the DLS analysis. Nevertheless, SHDS-treated HNPs (Fig. 3D') apparently underwent a dramatic transformation in terms of morphology with evident biological material surrounding the HNPs. Being soluble at acidic pH (Additional file 1: Fig S3) HNPs are expected to dissolve in the SGF [60], and eventually re-precipitate in the SIF.

On the other hand, LSNPs were likely subjected to hydrolysis by lipases [61]. To investigate the susceptibility of LSNPs to enzymatic degradation, this NBM was incubated in a solution of lipase in water at the same pH as the intestinal fluid, and the size distribution was monitored up to 24 h (Additional file 1: Fig S4). A shift of the  $d_H$  distribution towards lower values was observed already after 15 min (Additional file 1: Fig S4A) indicating degradation; a decrease of approximately 8% in the mean  $d_H$  value occurred after 24 h (Additional file 1: Fig S4B). These data confirm the partial degradation of LSNPs observed by TEM analysis (Fig. 3A').

#### Bio-molecular corona formation during SHDS

The formation of a bio-molecular corona was investigated on CNPs and FNPs, because these NBMs exhibit a surface reactivity that can be used as a probe to monitor the extent of coverage of the surface.

The SHDS was performed firstly with and without active components (proteins, bile and uric acid, Table 4), and the size distribution changes were monitored (Fig. 4).

In both SGF and SIF a higher Z-average and PDI values in the absence of active components was observed compared to fluids with active components. The suspensions were largely unstable, and the particles slowly deposited on the bottom of the flask, as shown in Fig. 4. This confirms the formation of a bio-molecular corona in the SHDS that stabilizes the colloids.

To gain information on the extent of the surface coverage, the NBMs were analysed for their surface charge by ELS and reactivity by electron paramagnetic resonance (EPR) spectroscopy (Fig. 5). The experiments were performed after washing steps aimed at removing the soft corona.

The  $\zeta$ -potential was measured in ultrapure water by varying the pH of the suspension (Fig. 5A and B). The  $\zeta$ -potential curves of CNPs treated with SHDS were different compared to untreated CNPs, suggesting the presence of biomolecules at the surface. Similarly, treated

(See figure on next page.)

**Fig. 2** Size distribution changes after incubation with the SHDS. Upper panels: DLS patterns of the NBMs in the different fluids of the SHDS; **A** LSNPs; **B** CNPs; **C** FNPs; **D** HNPs. Each line represents the mean values of 15 measurements that were obtained in three independent experiments. Lower panels: FPIA size distribution of the NBMs after SHDS; **E** LSNPs; **F** CNPs; **G** FNPs; **H** HNPs. The concentration is reported as the number of micrometric particles. Each line is the mean of three independent experiments  $\pm$  SD



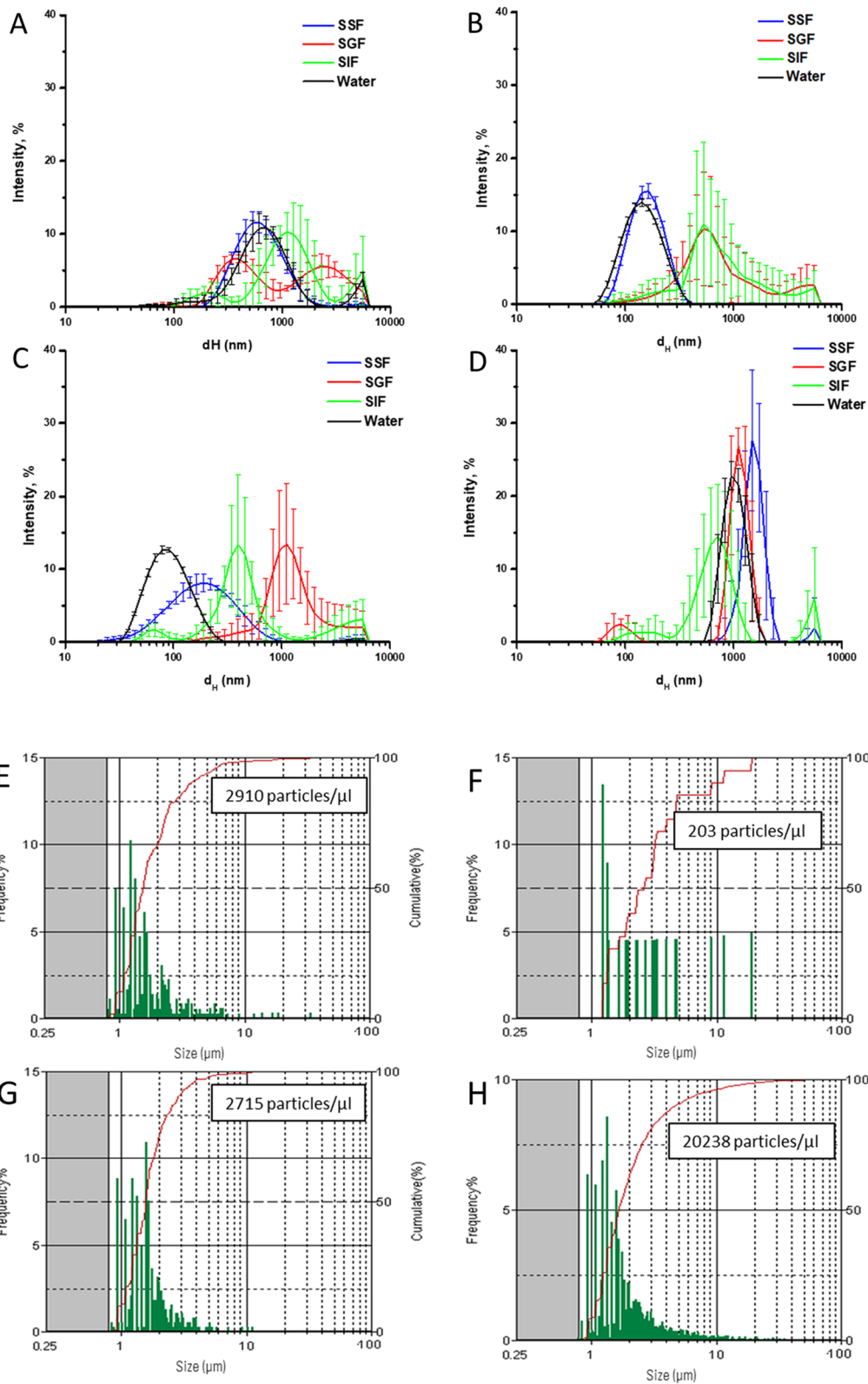


**Fig. 2** (See legend on previous page.)



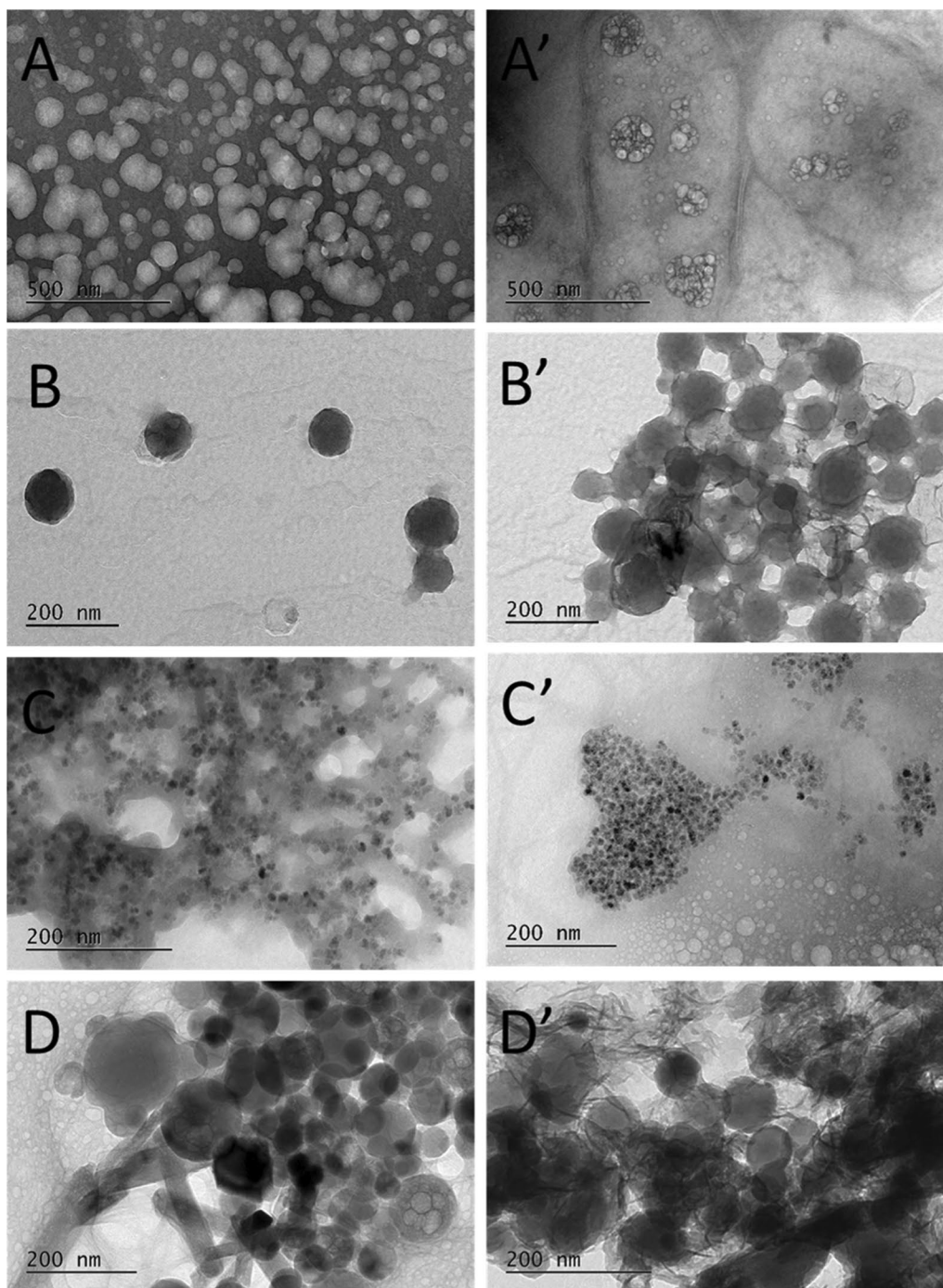


**Fig. 3** Transformation of NBMs monitored by TEM analysis. Representative TEM images of **A** LS NPs; **B** CNPs; **C** FNPs; **D** HNPs before SHDS-treatment and **A'** LS NPs; **B'** CNPs; **C'** FNPs; **D'** HNPs after SHDS-treatment

324 FNPs showed a  $\zeta$ -potential shift, which might be due to  
 325 the presence of a bio-molecular corona, and/or to the  
 326 removal of the polymeric coating.

327 The surface reactivity was monitored by using the  
 328 spin-probe TEMPONE-H. This is an unspecific probe

able to react with Reactive Oxygen Species with redox-  
 active surface centres leading to the stable radical TEM-  
 PONE, detectable by EPR spectroscopy [62]. Therefore,  
 this system is suitable to monitor the surface reactivity of  
 nanomaterials.

329  
 330  
 331  
 332  
 333

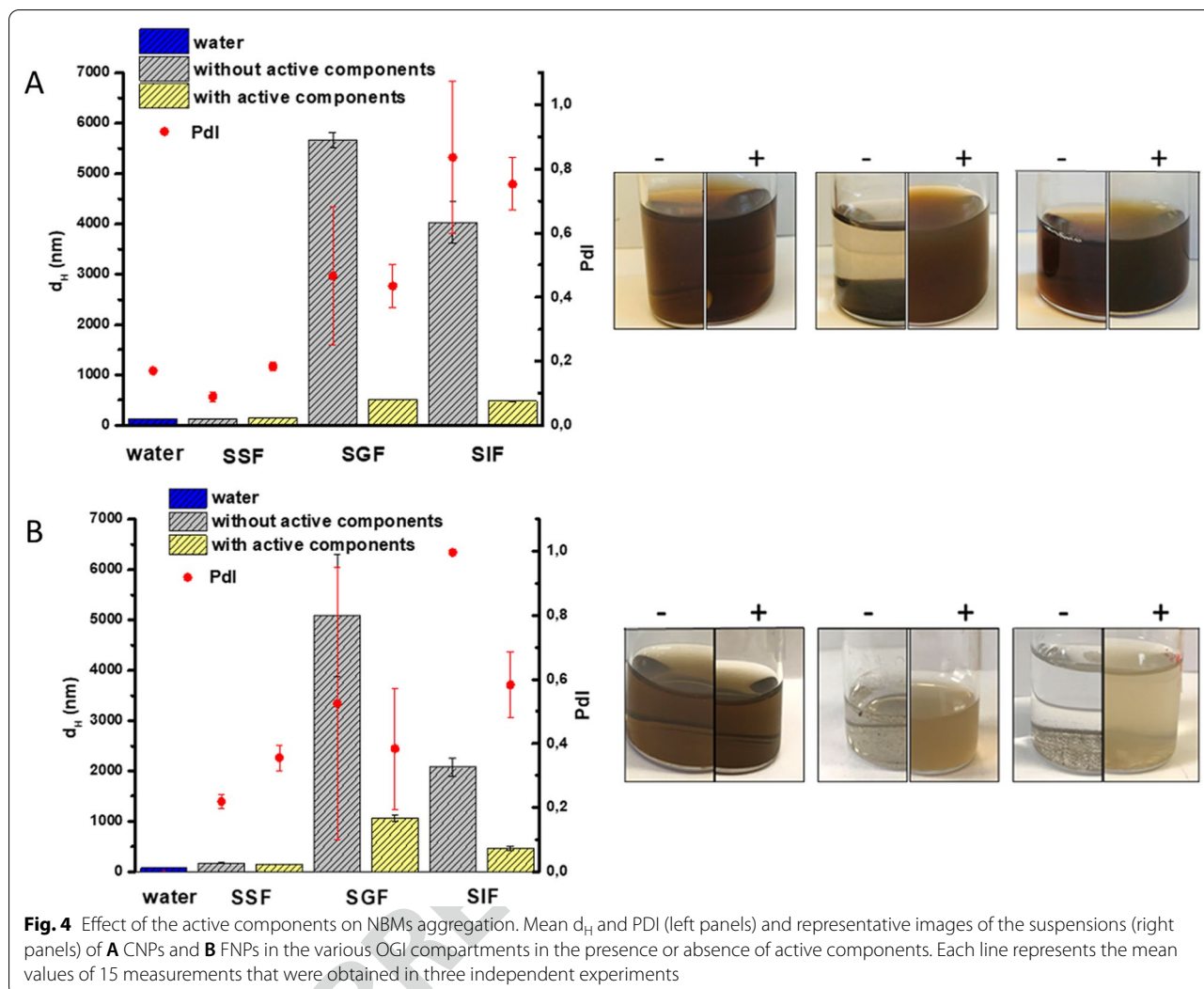


**Fig. 4** Effect of the active components on NBMs aggregation. Mean  $d_H$  and PDI (left panels) and representative images of the suspensions (right panels) of **A** CNPs and **B** FNPs in the various OGI compartments in the presence or absence of active components. Each line represents the mean values of 15 measurements that were obtained in three independent experiments

334 In the presence of untreated CNPs (Fig. 5A') or FNPs  
 335 (Fig. 5B'), the typical three-line signal of the TEMPONE  
 336 radicals was observed. When treated with SHDS the sur-  
 337 face reactivity of both FNPs and CNPs decreased, but  
 338 was not eliminated, suggesting that the surface was still  
 339 partially exposed to the solvent.

340 **NBMs identity in cell culture medium and in SHDS**

341 In vitro cellular tests require the use of cell medium,  
 342 which contains several components, including proteins.  
 343 During the NBM incubation in this medium, their bio-  
 344 logical identity may be further modified due to the parti-  
 345 cles interaction with the medium components. Therefore,  
 346 we firstly investigated any changes in the material size  
 347 distribution following exposure to protein rich fluid.  
 348 Fig 6 shows a comparison of treated and untreated  
 349 NBMs diluted in cell medium (Dulbecco's Modified Eagle  
 350 Medium (DMEM) with 10% Foetal Bovine Serum (FBS)).

The mean  $d_H$  values and PDI are reported in Additional  
 file 1: Table S1.

The NBMs exposure to the SHDS resulted in a dra-  
 matic change of the size distribution for all NBMs.

Treated LSNPs exposed to cell medium were more stable  
 over time than the untreated ones (Fig. 6A), but they  
 displayed a wider range of size, with a population char-  
 acterised by a mean diameter smaller than the LSNPs  
 in water, likely as a consequence of a partial degrada-  
 tion. Both treated and untreated CNPs were stable in cell  
 medium up to 24 h (Fig. 6B). A moderate shift of the sizes  
 towards values higher than the particles in water was  
 however observed, more evident for the treated CNPs.  
 A visible time-dependent instability in cell medium was  
 observed for both treated and untreated FNPs (Fig. 6C)  
 and HNPs (Fig. 6D). Treated FNPs were largely aggre-  
 gated in cell medium, while a moderate shift of the curve  
 towards higher  $d_H$  was observed for the untreated FNPs

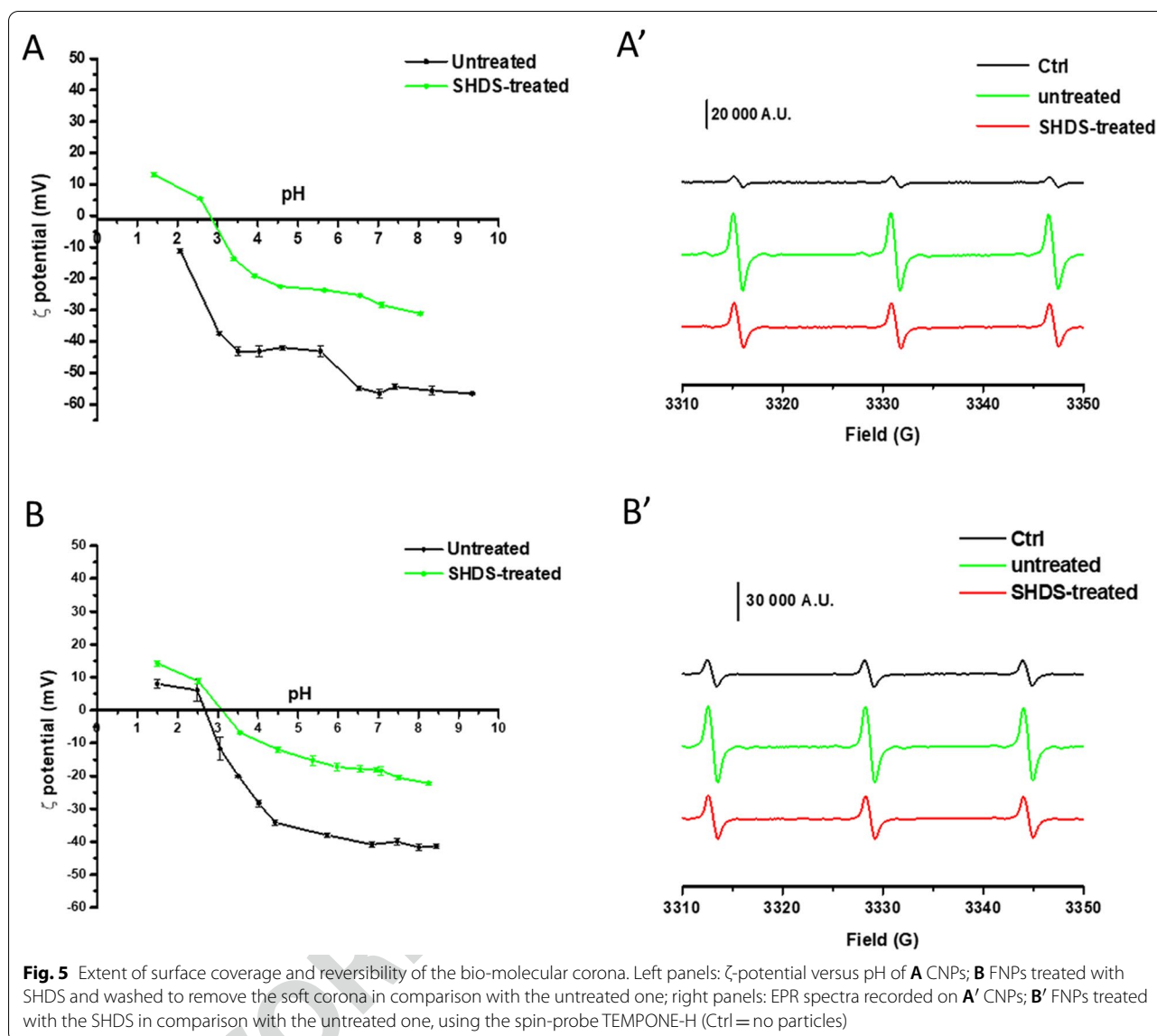


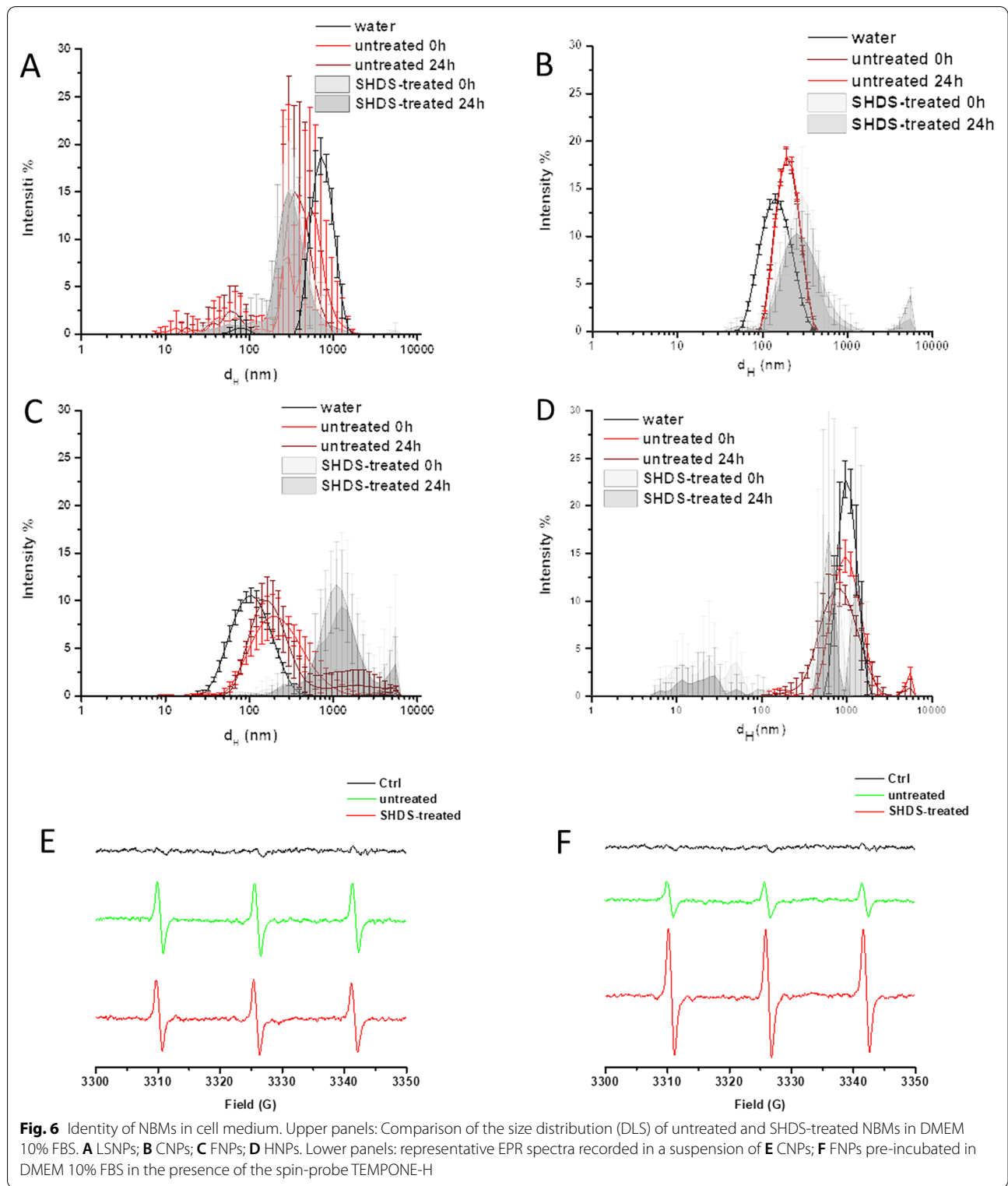
**Fig. 5** Extent of surface coverage and reversibility of the bio-molecular corona. Left panels:  $\zeta$ -potential versus pH of **A** CNPs; **B** FNPs treated with SHDS and washed to remove the soft corona in comparison with the untreated one; right panels: EPR spectra recorded on **A'** CNPs; **B'** FNPs treated with the SHDS in comparison with the untreated one, using the spin-probe TEMPONE-H (Ctrl=no particles)

369 in comparison to water. Untreated HNPs appeared to  
 370 form slightly more stable colloids in cell medium than in  
 371 water; while after SHDS several populations with a wide  
 372 range of size appeared. The formation of aggregates of  
 373 size above the detection limit of DLS was clearly visible  
 374 for all NBMs in cell medium (Additional file 1: Fig S5).

375 The surface reactivity of CNPs and FNPs in the cell  
 376 medium was also monitored by EPR spectroscopy  
 377 (Fig. 6E and F). Both treated and untreated CNPs had  
 378 similar surface reactivity in cell medium, suggesting that  
 379 the surface of the particles is still exposed to the solvent.  
 380 In the case of FNPs, the SHDS-treated sample exhibited  
 381 an unexpectedly high surface reactivity, likely caused by  
 382 the presence in the bio-molecular corona of some redox-  
 383 active components.

384 The hard protein corona composition was also analysed  
 385 for treated and untreated NBMs after incubation in cell  
 386 medium. For the isolation of the corona-NBM complex,  
 387 three steps of centrifugation were necessary to remove  
 388 the soft corona [63]. However, a protein background was  
 389 detected for the control sample, only composed by SHDS  
 390 and DMEM 10% FBS and no NBMs (Additional file 1:  
 391 Fig S6E), suggesting that the digestion process and the  
 392 long incubation time led to protein aggregation. Unfor-  
 393 tunately, it was not possible to discriminate the protein  
 394 corona from the background proteins that co-precipitated  
 395 during the NBMs-corona isolation protocol. Thus, we  
 396 studied the effect of the treatment with SHDS only for  
 397 FNPs. In fact, for these NBMs a magnetic separation was  
 398 used as an alternative method to remove the soft corona.





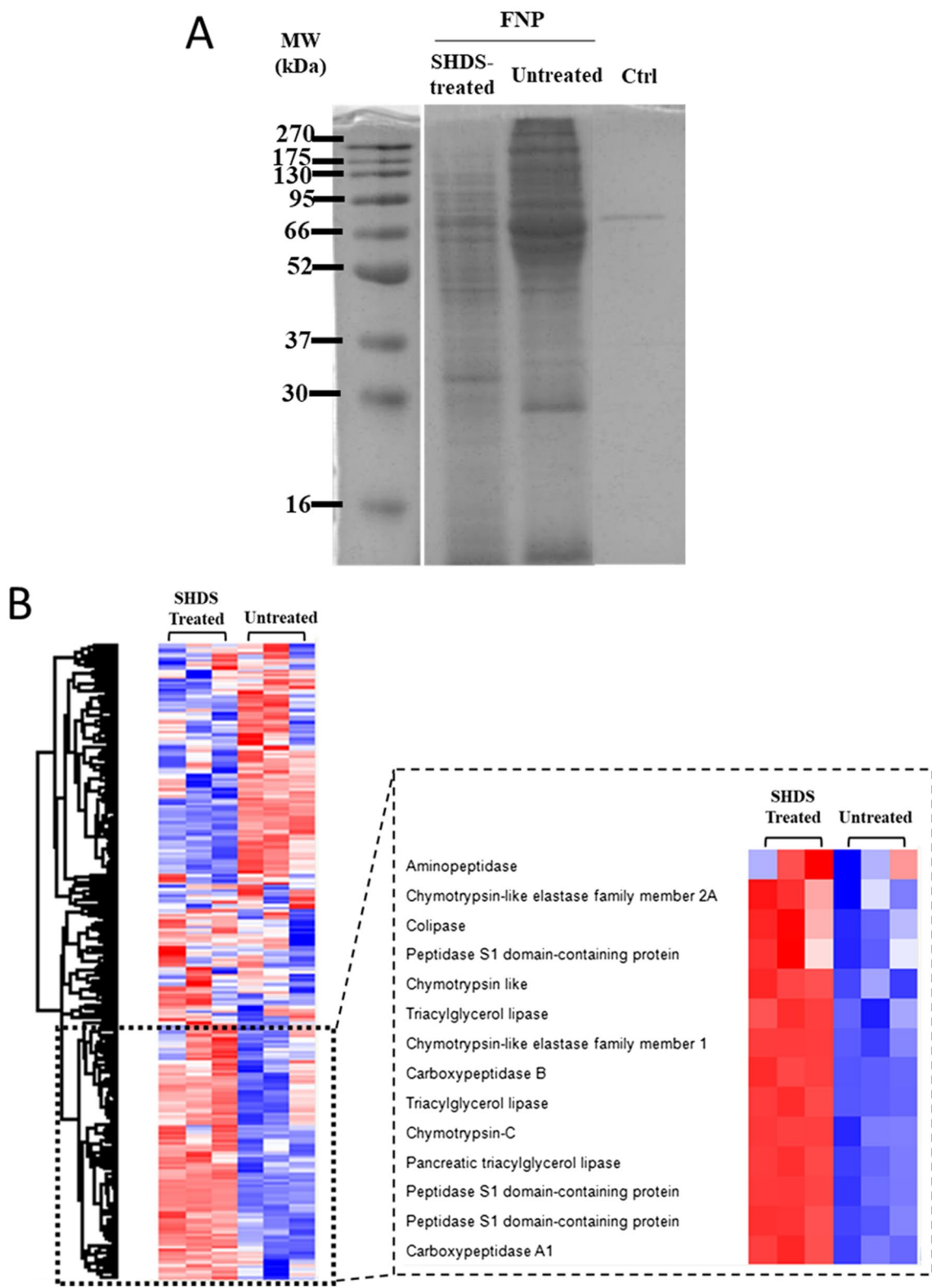


**Fig. 7** Effect of the SHDS on the protein corona composition of FNPs incubated in DMEM 10% FBS for 24 h. **A** SDS-PAGE analysis (Ctrl = SHDS + DMEM 10% FBS without FNPs). **B** Heat map showing the relative abundance for each protein normalizing the mean value for the same protein. Proteins derived by SHDS are highlighted in the square

399 In Fig. 7A the SDS-PAGE analysis of the hard corona is  
400 shown. Clearly, the treatment with SHDS affected the  
401 corona composition since treated and untreated samples  
402 had different protein patterns.

403 Proteomic analysis by mass spectrometry for these  
404 samples identified more than 200 proteins for the corona  
405 of both SHDS-treated and untreated FNPs (Fig. 7B).

The top 20 most abundant proteins are listed in Table 2.  
Label free quantification (LFQ) calculated with Perseus  
was used to compare the protein abundance between the  
two samples.

Within the top 20 most abundant proteins, some serine  
proteases derived from SHDS were found in the SHDS  
treated sample. Different chymotrypsins derived from

406  
407  
408  
409  
410  
411  
412

**Table 2** Top 20 most abundant proteins for SHDS-treated and untreated FNPs

	FNP SHDS + DMEM 10% FBS				FNP DMEM 10% FBS			
	LFQ ± SEM (x1E08)	Protein Name	Protein ID	MW (kDa)	LFQ ± SEM (x1E08)	Protein Name	Protein ID	MW (kDa)
1	12.4 ± 3.4	Bovine Alpha-2-HS-glycoprotein*	P12763	38.4	8.11 ± 1.6	Bovine Haemoglobin foetal subunit beta*	P02081	15.9
2	12.3 ± 1.8	Bovine Alpha-1-anti-proteinase*	P34955	46.1	4.81 ± 0.19	Bovine Alpha-1-anti-proteinase*	P34955	46.1
3	10.0 ± 0.90	Pig Peptidase S1 domain-containing protein**	I3LHI7	27.7	3.99 ± 0.050	Bovine Alpha-2-HS-glycoprotein*	P12763	38.4
4	7.96 ± 0.32	Bovine Albumin*	P02769	69.3	3.27 ± 0.34	Bovine Albumin*	P02769	69.3
5	6.84 ± 1.1	Bovine Haemoglobin foetal subunit beta*	P02081	15.9	3.22 ± 0.70	Bovine Haemoglobin subunit alpha*	P01966	15.2
6	4.03 ± 0.60	Bovine Apolipoprotein A-I*	P15497	30.3	2.67 ± 0.35	Bovine Apolipoprotein A-I*	P15497	30.3
7	3.42 ± 0.76	Bovine Histone H2A type 2-C	A1A4R1	14	2.45 ± 0.11	Bovine Inter-alpha-trypsin inhibitor heavy chain H2*	A0A3Q1LK49	96.8
8	2.45 ± 0.24	Bovine Haemoglobin subunit alpha*	P01966	15.2	2.35 ± 0.35	Bovine Angiotensinogen*	P01017	51.4
9	2.43 ± 0.35	Pig Triacylglycerol lipase**	F1S4T9	51.6	2.04 ± 0.18	Bovine Alpha-fetoprotein*	Q3SZ57	68.6
10	2.42 ± 0.35	Pig HATPase_c domain-containing protein**	A0A287A9T4	83	1.90 ± 0.16	Bovine Apolipoprotein A-II*	P81644	11.2
11	2.32 ± 0.57	Bovine Serpin family G member 1	E1BMJ0	51.8	1.88 ± 0.14	Bovine Inter-alpha-trypsin inhibitor heavy chain H4	F1MMD7	101.5
12	2.26 ± 0.42	Pig Carboxypeptidase A1**	P09954	47.2	1.87 ± 0.10	Bovine Alpha-1-microglobulin	F1MMK9	53
13	2.02 ± 0.80	Bovine Angiotensinogen*	P01017	51.4	1.80 ± 0.17	Bovine Beta-2-glycoprotein 1*	P17690	38.3
14	2.00 ± 0.13	Bovine Alpha-fetoprotein*	Q3SZ57	68.6	1.54 ± 0.090	Bovine Alpha-2-macroglobulin	Q7SIH1	167.6
15	1.61 ± 0.85	Bovine Histone H2A	F2Z4G5	14.1	1.52 ± 0.15	Bovine Fetuin-B	Q58D62	42.7
16	1.58 ± 0.10	Bovine Beta-2-glycoprotein 1*	P17690	38.3	1.46 ± 0.24	Bovine Vitronectin*	Q3ZBS7	53.6
17	1.58 ± 0.10	Bovine Inter-alpha-trypsin inhibitor heavy chain H2*	A0A3Q1LK49	96.8	1.46 ± 0.037	Bovine Complement C3	Q2UVX4	187.3
18	1.39 ± 0.16	Bovine Apolipoprotein A-II*	P81644	11.2	1.39 ± 0.12	Bovine Alpha-1B-glycoprotein	Q2KJF1	53.6
19	1.30 ± 0.19	Pig Peptidase S1 domain-containing protein**	I3LJ52	26.9	1.28 ± 0.11	Bovine Inter-alpha-trypsin inhibitor heavy chain H3	P56652	99.6
20	1.14 ± 1.7	Bovine Vitronectin*	Q3ZBS7	53.6	1.28 ± 0.11	Bovine Complement factor B	P81187	85.4

\* Common proteins; \*\*proteins from SHDS. LFQ was calculated with Perseus (n = 3). SEM refer to the standard error of the mean for n = 3



pancreatin were also detected among the less abundant proteins (data not shown). On the other hand, proteins highly abundant in FBS [64], were found in the corona for both samples, in particular alpha-2-HS-glycoprotein, apolipoprotein AI and AII, bovine haemoglobin alpha and beta chain, and alpha-1-antiproteinase. This latter, alpha-1-antiproteinase, also known as alpha-1-anti-trypsin, alpha-1-proteinase inhibitor or serpin A1, is an inhibitor of serine proteases. A comparison of the abundance of proteases in treated and untreated samples is shown in Additional file 1: Fig S7.

#### Effects of SHDS on the cytotoxicity toward epithelial intestinal Caco-2 cells, HCT116 cells and primary human colonic epithelial cells

To investigate the effect of SHDS treatment on the NBMs cytotoxicity, a dose-dependent viability assay in Caco-2 and HCT116 cells, using a dose range from 0 to 150 µg/ml was performed.

This range was chosen based on the toxicity given by the OGI fluids alone tested at the same dilutions used for NBMs. Indeed, preliminary experiments indicated that OGI fluids were not significantly toxic up to dilution corresponding to 150 µg/ml NBMs (Additional file 1: Fig S8A).

In both Caco-2 and HCT116 cells, a very low toxicity was observed for untreated LSNPs up to 100 µg/ml. However, after the treatment with SHDS a significant cytotoxicity was observed for concentrations higher than 75 µg/ml and 20 µg/ml in Caco-2 and HCT116 cells, respectively (Fig. 8A). On the contrary, neither SHDS-treated nor untreated CNPs were toxic and SHDS did not alter the profile of toxicity of this NBM in both cell lines (Fig. 8B). On Caco-2 cells, untreated FNPs displayed the highest cytotoxicity, starting at 10 µg/ml, but in contrast with the other NBMs, SHDS has a cytoprotective effect: indeed, SHDS-treated FNPs became toxic at 50 µg/ml and were significantly less toxic than untreated ones in the range 50–75 µg/ml (Fig. 8C). A similar effect of toxicity masking was observed for HNPs: indeed, untreated HNPs were toxic from 50 µg/ml, but after SHDS no toxicity was detected at all the concentrations tested. As further confirmation, SHDS-treated HNPs were significantly less cytotoxic than untreated ones (Fig. 8D). On HCT116 cells, neither untreated nor SHDS-treated FNPs and HNPs induced any significant cytotoxicity (Fig. 8C and D).

Caco-2 and HCT116 cells are widely used as models of gastrointestinal cells [65]. However, being immortalized, they are expected to be more resistant to external stimuli. Therefore, we measured the effect of NBMs also in primary non-transformed intestinal epithelial cells (HCoEpiC). In general, all the NBMs showed toxicity at

lower concentrations than on Caco-2 and HCT116 cells (Fig. 9). This finding can be partially explained by the higher sensitivity of HCoEpiC to SHDS fluids, which are toxic at a lower concentration (50 µg/ml) (Additional file 1: Fig S8B) than in immortalized cells (Additional file 1: Fig S8A). On this basis, we decided to evaluate the NBMs at a concentration range (2.5–20 µg/ml) immediately below the first toxic concentration for SHDS fluids.

The pre-incubation with SHDS increased the cytotoxicity of LSNPs and CNPs (Fig. 9A and B). We did not detect any significant cytotoxicity changes between SHDS-treated and untreated FNPs (Fig. 9C), while HNPs were the only NBM showing lower cytotoxicity after SHDS towards both Caco-2 (Fig. 8D) and HCoEpiC cells (Fig. 9D).

These data show a different behaviour on epithelial intestinal cells in relation to the nature of NBMs that can undergo different modifications during SHDS. Moreover, the choice of in vitro model to evaluate cytotoxicity is also of paramount importance, as demonstrated by the different sensitivity between Caco-2 cells, HCT116 cells and primary non-transformed cells.

The genotoxicity of NBMs was then evaluated on HCT116 cells because, although it is a cancer-derived cell line, it bears wild-type p53 contrarily to Caco-2 cells. None of the tested NBM induced any significant increase of DNA strand breaks as assessed by counting 53BP1 DNA repair foci, while the positive control, i.e., cells exposed for 24 h to 50 µM etoposide, led to a statistically significant increase of 53BP1 foci count (Additional file 1: Fig S9).

#### Effects of SHDS on viability and permeability of Caco-2 intestinal barrier model

Finally, we investigated the effects of NBMs on viability, permeability, and inflammation parameters in a competent model of GI barrier, i.e. the 21-day differentiated Caco-2 model.

When Caco-2 cells grow on specific inserts and reach the complete confluence, they begin to differentiate, completing the process after 21 days [66]. This model is recognized as a valid GI barrier model, widely used in permeability assessment tests because it mimics intestinal physiology [67, 68]. Thus, we used this model to investigate the effects on cell viability and barrier permeability for all SHDS-treated and untreated NBMs. Since there are no literature data about the physiological doses in patients exposed to these NBMs but at the same time there are also no reports of severe acute toxicity, we decided to study the highest non-toxic dose of NBMs for Caco-2 undifferentiated cells, to highlight the differences in terms of toxicological properties of NBMs, before and after the simulated digestive process. Barrier-forming



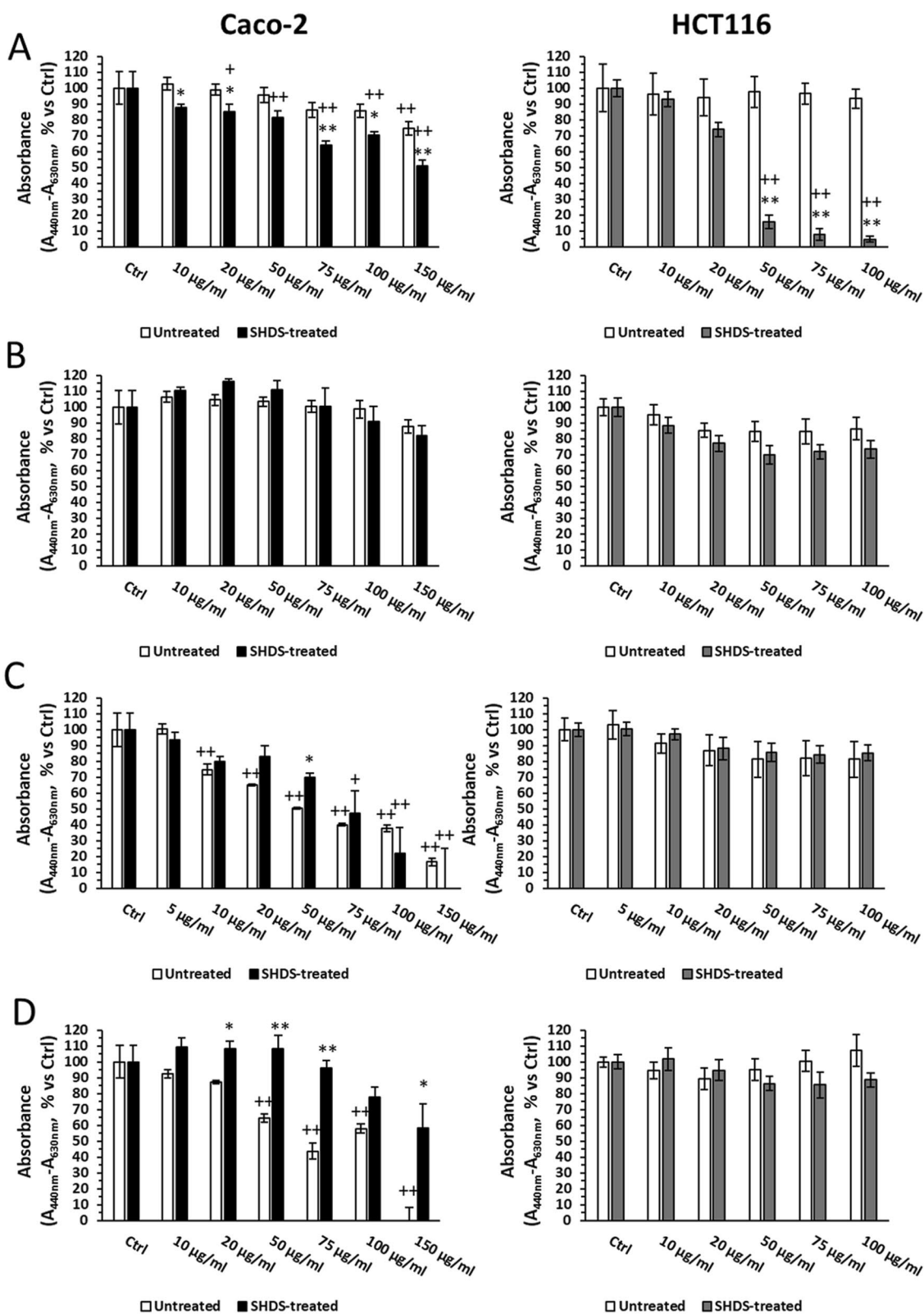
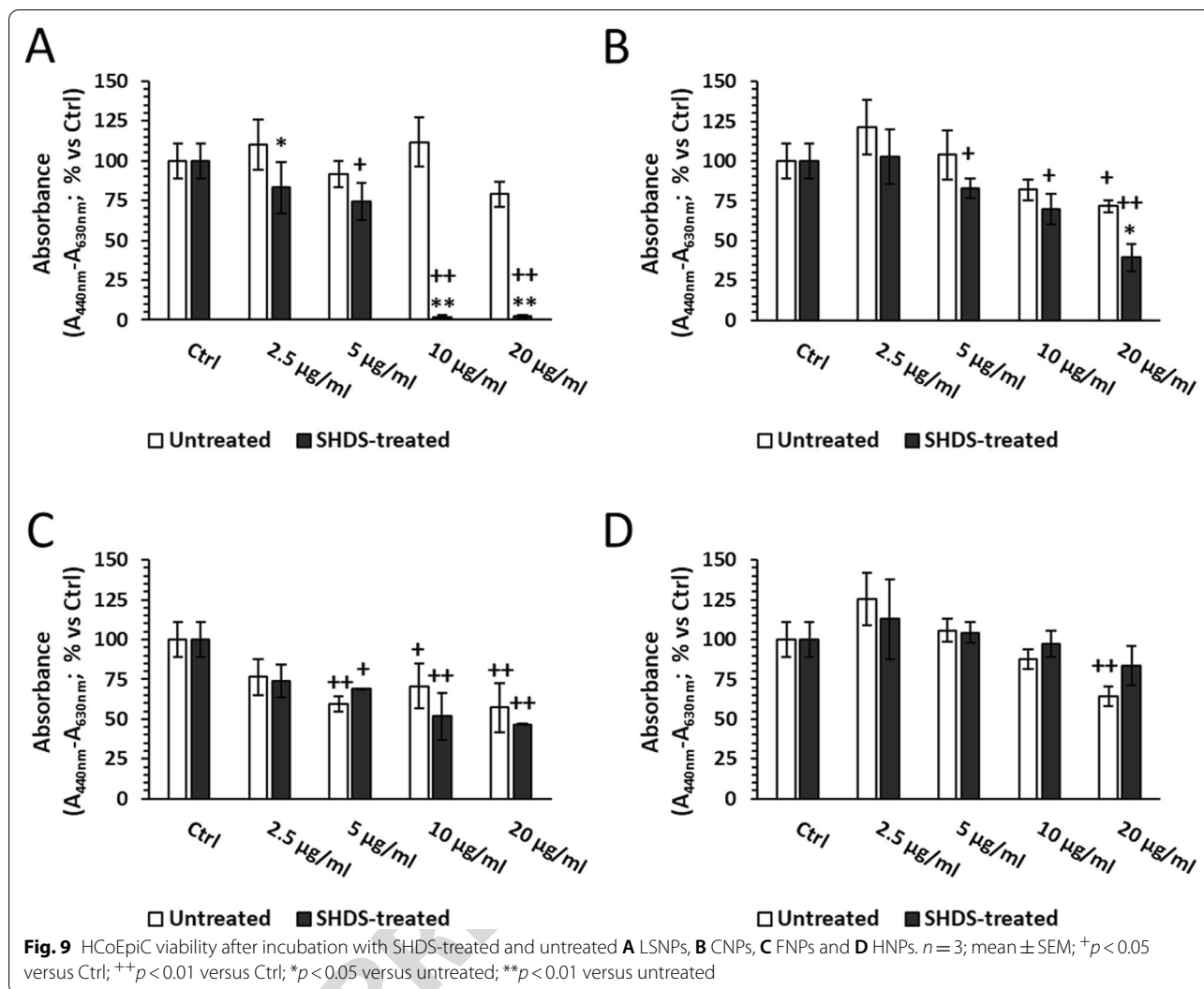


**Fig. 8** Cell viability of Caco-2 (left) and HCT116 (right) cells after incubation with SHDS treated and untreated **A** LSNPs, **B** CNPs, **C** FNPs and **D** HNPs. *n* = 3; mean ± standard error (SEM); +*p* < 0.05 versus Ctrl; ++*p* < 0.01 versus Ctrl; \**p* < 0.05 versus untreated; \*\**p* < 0.01 versus untreated





517 cells were thus incubated for 24 h at the highest non-  
 518 toxic concentrations of SHDS-treated NBMs (150 µg/ml  
 519 for CNPs and HNPs and 50 µg/ml for LSNPs and FNPs)  
 520 (Fig. 8, left panel).

521 In the viability assays, neither untreated nor SHDS-  
 522 treated NBMs showed toxicity (Fig. 10A). Since toxic  
 523 effects of NBMs may alter barrier integrity and produce  
 524 inflammation [30], we next evaluated integrity param-  
 525 eters, in terms of functional assays, TEER and TJ levels,  
 526 and pro/anti-inflammatory cytokines production.

527 In our model, the absence of toxicity was paralleled  
 528 by the absence in permeability variation, measured by  
 529 the Lucifer Yellow permeability assay (Fig. 10B; Table 3).  
 530 Moreover, the TEER values were always > 600 Ω·cm<sup>2</sup> in  
 531 both untreated and NBM-treated barriers (Additional  
 532 file 1: Table S2).

533 Notably, each NBM increased one or more genes  
 534 involved in TJs with a specific pattern (Fig. 11). Untreated

LSNPs, FNPs and HNPs down-regulate occludin (OCLN) 535  
 (Fig. 11B) and to a lesser extent zonula occludens-1 536  
 (TJP1) (Fig. 11A), claudin 3 (CLDN3) (Fig. 11C) and clau- 537  
 din 5 (CLDN5) (Fig. 11D) genes. SHDS-treated LSNPs 538  
 increased only TJP1 and CLDN5, SHDS-treated FNPs 539  
 increased TJP1, OCLN and CLDN5, SHDS-treated HNPs 540  
 increased the expression of all these genes, although to a 541  
 different extent. Interestingly, CNPs were the only NBM 542  
 that increased the expression of all TJs-encoding genes 543  
 evaluated both in the untreated (except for CLDN5) and 544  
 in the SHDS-treated form (Fig. 11). 545

This up-regulation of TJs genes may suggest a compen- 546  
 satory response mounted by GI cells in response to 547  
 potentially cytotoxic NBMs. According to the functional 548  
 results in terms of permeability (Fig. 10B), such response 549  
 was successful in preventing the loss of barrier integrity. 550

Finally, we analysed the gene expression of TNF-α 551  
 and IL-6, two pro-inflammatory cytokines involved in 552

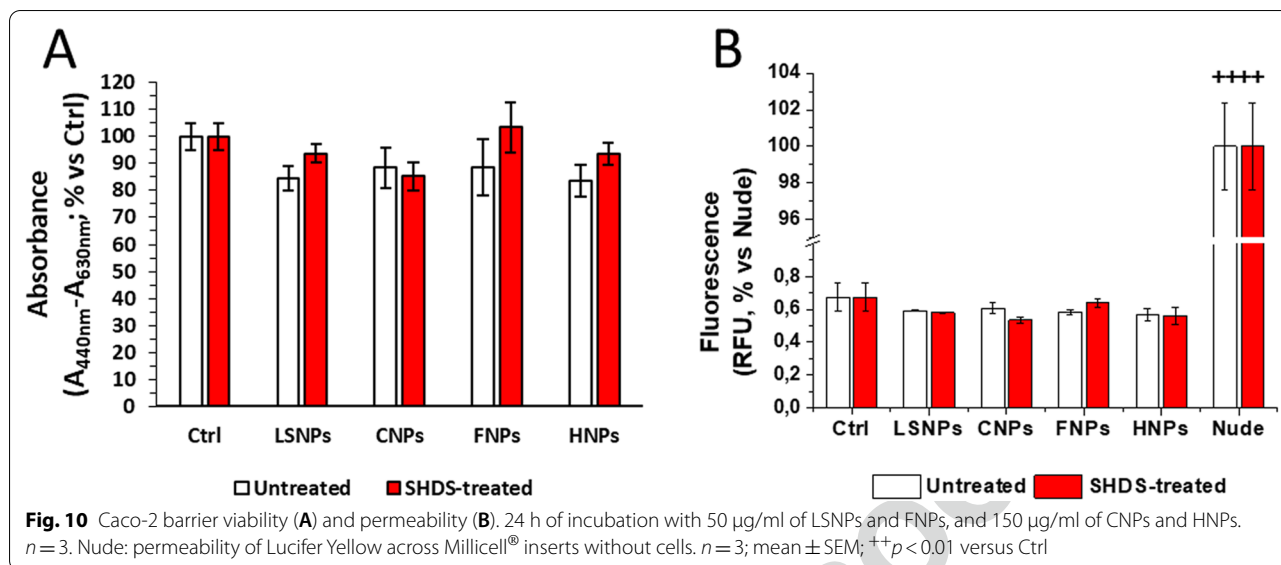


**Table 3** Apparent permeability (Papp) values of Caco-2 barrier model after 24 h of incubation

	Untreated Papp (cm/s)	SHDS-treated Papp (cm/s)
Ctrl	$2.61 \times 10^{-7} \pm 2.71 \times 10^{-8}$	$2.67 \times 10^{-7} \pm 1.40 \times 10^{-8}$
LSNPs	$2.32 \times 10^{-7} \pm 5.60 \times 10^{-9}$	$2.26 \times 10^{-7} \pm 3.20 \times 10^{-9}$
CNPs	$2.38 \times 10^{-7} \pm 1.83 \times 10^{-8}$	$2.09 \times 10^{-7} \pm 3.37 \times 10^{-9}$
FNPs	$2.29 \times 10^{-7} \pm 1.08 \times 10^{-8}$	$2.50 \times 10^{-7} \pm 1.35 \times 10^{-8}$
HNPs	$2.21 \times 10^{-7} \pm 9.92 \times 10^{-9}$	$2.18 \times 10^{-7} \pm 1.45 \times 10^{-8}$

24 h of incubation with 50 µg/ml of LSNPs and FNPs, and 150 µg/ml of CNPs and HNPs. *n* = 3; mean ± SEM

553 the pathogenesis of inflammatory bowel disease [69],  
 554 opposed to IL-10, known for its immune-suppressive role  
 555 in inflammatory bowel disease [70], and to IL-22, which  
 556 triggers regeneration after intestinal injuries [71] and  
 557 preserves the intestinal epithelial integrity [72].

558 None of the untreated NBMs significantly increased  
 559 the cytokines gene expression (Fig. 12), in line with the  
 560 low modulation of TJ-genes (Fig. 11). SHDS-treated  
 561 CNPs did not increase the expression of pro-inflamma-  
 562 tory TNF, which was instead increased by SHDS-treated  
 563 LSNPs, FNPs and HNPs (Fig. 12A). All the SHDS-  
 564 treated NBMs increased IL6 (Fig. 12B), but they also up-  
 565 regulated the anti-inflammatory/immune-suppressive  
 566 cytokines IL10 (Fig. 12C) and IL22 (Fig. 12D), suggesting  
 567 a balance between pro-inflammatory and anti-inflamma-  
 568 tory processes that could contribute to preserve the GI  
 569 barrier integrity.

570 **NBM intestinal barrier crossing**

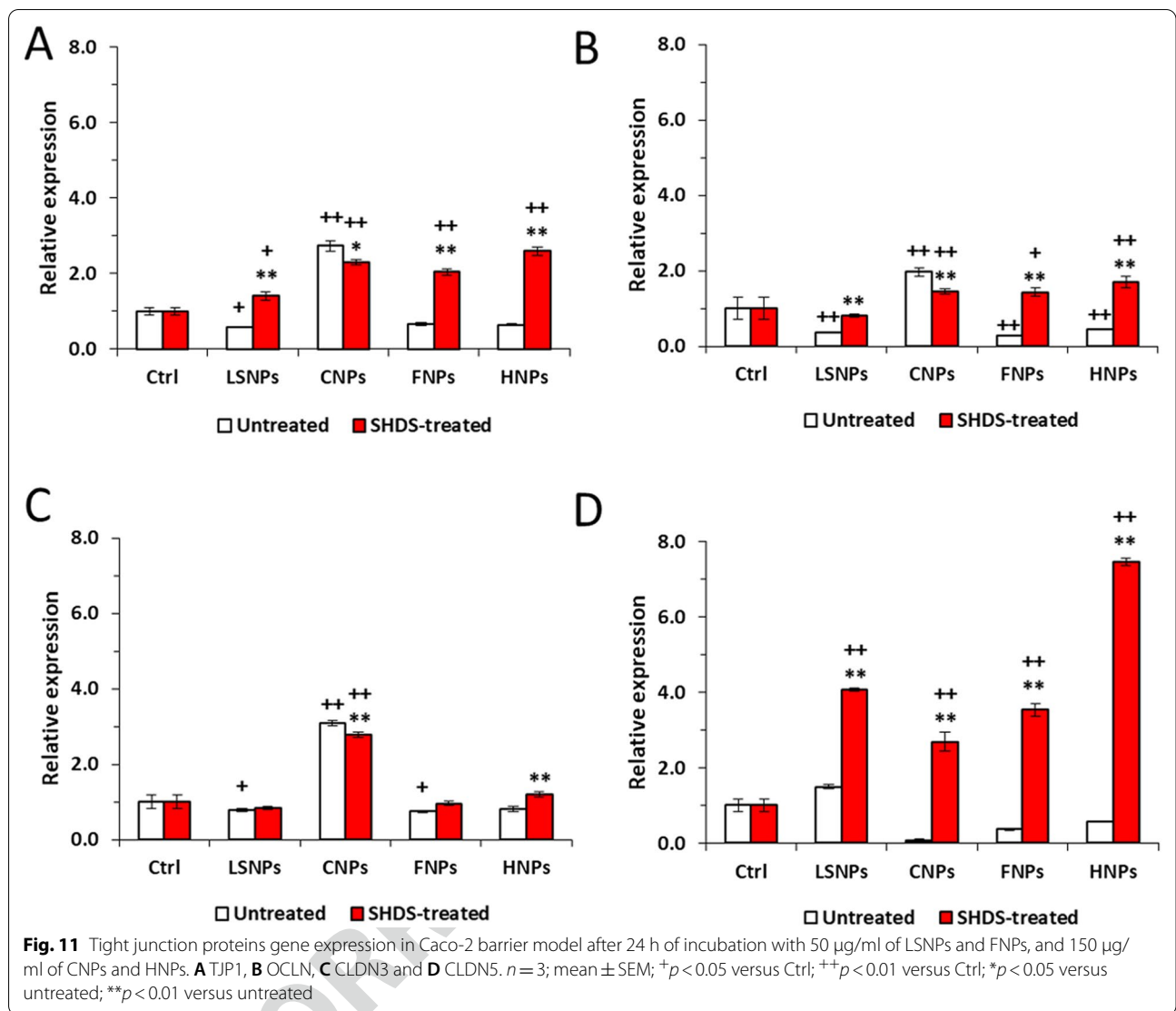
571 The results obtained with the Lucifer Yellow test sug-  
 572 gested that the tested NBMs are unable to cross the

barrier, even after SHDS-treatment. To monitor the  
 NBM possible transcellular translocation, the barrier  
 model was exposed to CNPs and FNPs and the particle  
 concentration in the basolateral compartment of Caco-2  
 GI barrier was monitored by Nanoparticle Track Analysis  
 (NTA). These samples were selected because the techni-  
 que is more sensible on samples with a highly refractive  
 index. No particles were found in the basolateral com-  
 partment after treatment with both SHDS-treated and  
 untreated CNPs and FNPs (data not shown). These data  
 were confirmed for FNPs using the FerroZine™ assay  
 which showed no significant presence of iron (data not  
 shown).

**Discussion**

The exposure to NBMs is becoming more and more com-  
 mon due to their widespread use in various industrial  
 sectors including food and medicine. Consequently, the  
 number of studies focusing on NBMs hazard are increas-  
 ing exponentially [73–75]. Ingestion has been recognized  
 as an important route of exposure to both nanomaterials  
 and NBMs only recently. For this reason it has been lit-  
 tle investigated so far. Moreover, because of the complex-  
 ity of the OGI tract physiology, a consensus on the most  
 suitable models and markers for the assessment of NBM  
 toxicity has not been reached yet.

Recently, several cellular models have been proposed  
 to mimic the manifold gut anatomy and physiology [32,  
 33, 76–79]. However, in most of the existing studies cells  
 are exposed to untreated NBMs, neglecting the trans-  
 formations that occur to NBMs during the transit in the  
 OGI tract [13]. Recently, different in vitro systems sim-  
 ulating digestion have been proposed to monitor such



605 biotransformation [50, 80, 81]. Nevertheless, few studies  
 606 have been published on the impact that the NBM bio-  
 607 transformation along the OGI tract may have on their  
 608 toxicity toward intestinal cells [39, 52–54, 82].

609 In the present study we found that the application of  
 610 an in vitro Simulated Human Digestion System (SHDS)  
 611 induces a significant modification of the bioidentity of  
 612 four NBMs, which in turn modulates their bioactivity  
 613 towards intestinal epithelial cells. Samples representative  
 614 of NBMs with potential applications in oral drug delivery  
 615 (FNPs, CNPs, HNPs, LSNPs) [55–58] or as ingredients of  
 616 nutraceutical formulations have been selected (LSNPs)  
 617 [83].

618 **NBMs acquire a new identity in the OGI tract**

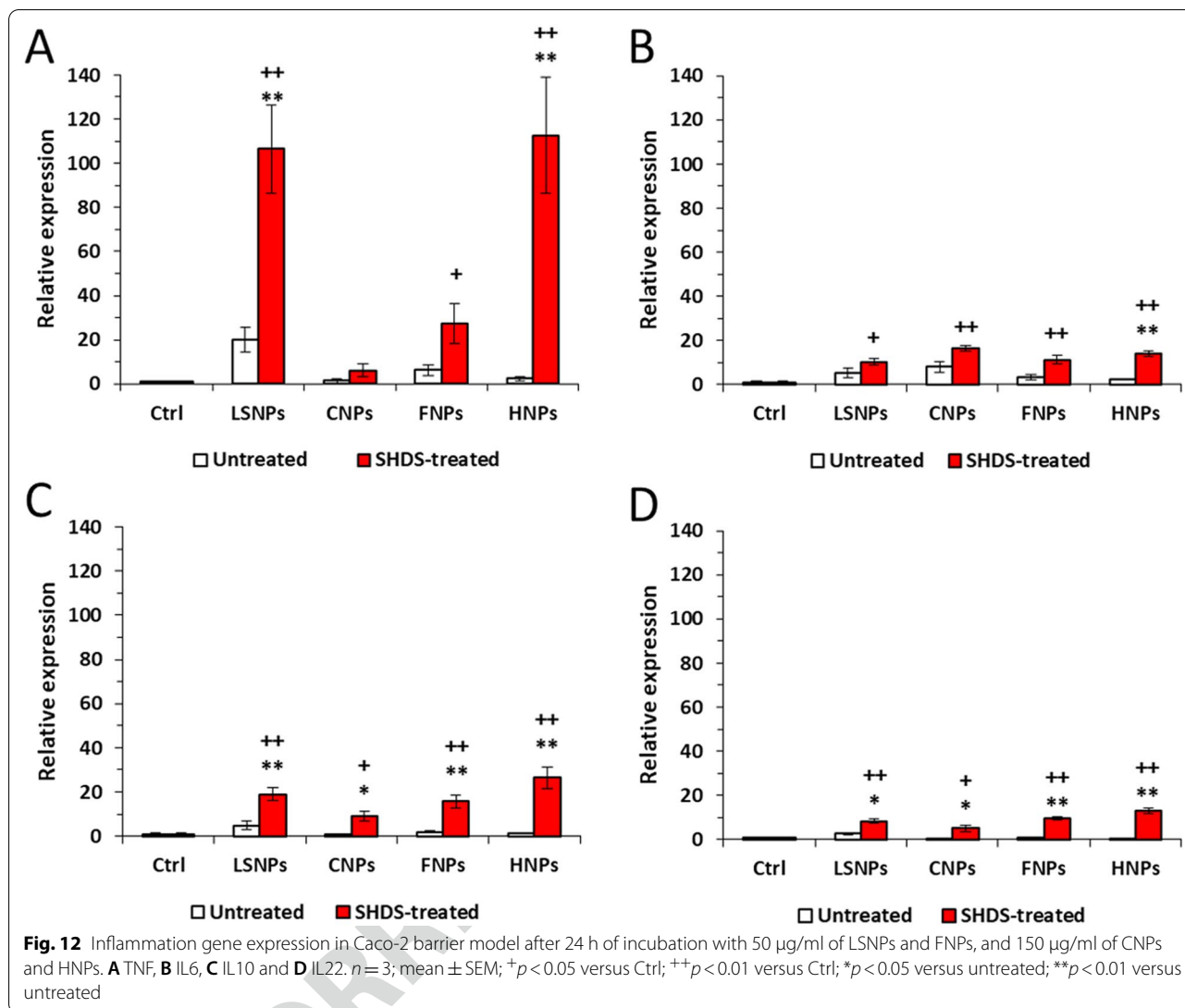
619 The concept that the NBM bioactivity strongly depends  
 620 upon their physical and chemical properties is currently

well consolidated. Size and surface properties are the  
 parameters which have been recognized to modulate the  
 NBM toxicity [84–86].

Size primarily affects dosimetry and cellular uptake.  
 Smaller particles can penetrate cells more easily by active  
 processes such as caveolae- and clathrin-mediated endo-  
 cytosis, or by passive diffusion across the cell membrane  
 [87]. On the other hand, size affects particle sedimenta-  
 tion and diffusion, thus modifying the kinetics of contact  
 with cells and the effective dose [88, 89].

An increase of the particles size consequent to aggre-  
 gation or agglomeration following contact with simulated  
 gastric or intestinal fluids has been previously reported  
 for several types of NBMs, as lipid nanoparticles [90], Ag  
 nanoparticles [52, 91, 92], TiO<sub>2</sub> nanoparticles [39, 93],  
 silica nanoparticles [52, 94], amorphous Mg-Ca phos-  
 phate nanoparticles [95], Au nanoparticles [96], and





638 others [97, 98]. Our study confirms previous reports, 639 since a significant increase of the size has been observed 640 for all the NBMs investigated (Fig. 2). More importantly, 641 we demonstrate that this process, occurring mainly in 642 the gastric compartment, is irreversible regardless of the 643 chemical composition of the NBMs. In fact, all NBMs 644 appear aggregated in the cell media, and in these forms 645 have a higher probability to interact with the intestinal 646 cells in vivo. The low pH and the high ionic strength of 647 the gastric fluid are the main driving force of aggregation, 648 as demonstrated for stabilized zero-valent iron nanoparticles [99] and Au nanoparticles [100], while proteins in 649 the medium appear to partially inhibit the process. 650 However, aggregation is not the only transformation 651 process that NBMs undergo. In fact, in the case 652 of HNPs, LSNPs and FNPs the aggregates appear composed 653 of particles smaller than the untreated ones. 654

Dissolution, enzymatic degradation or coating degradation 655 were observed, in line with other studies reporting 656 that extreme pH can dissolve pH-sensitive NBMs [101], 657 and that enzymes and proteins can contribute to NBMs 658 dissolution by digesting NBMs components [102]. 659 Another important aspect is the modification of the 660 NBMs surface chemistry. Surface charge both affects 661 colloidal stability and nanoparticles-membrane interaction 662 [103–105]. On the other hand, the NBM surface 663 acts as a scaffold that binds proteins and biomolecules, 664 leading to the acquisition of a new biological identity 665 [106–110] that influences the NBMs affinity for different 666 cell types and specific receptors [51, 87]. The 667 composition of bio-molecular corona and subsequent 668 NBMs activity strongly depend on the specific bio-fluid 669 in which they are dispersed [111–114]. 670

671 Our study clearly shows that proteins and other com- 723  
672 ponents (e.g., bile salts) can irreversibly bind to the sur- 724  
673 face by forming a hard corona. Clear-cut differences in 725  
674 the bio-molecular corona were found between untreated 726  
675 FNPs and SHDS-treated FNPs. Indeed, SDS-PAGE and 727  
676 mass spectrometry identified different proteases derived 728  
677 from SHDS. This corona also partially protects HNPs 729  
678 and LSNPs from degradation. The protective effect of 730  
679 proteins has been previously observed for hydroxyapa- 731  
680 tite nanoparticles after the addition of milk to the in vitro 732  
681 digestive process, resulting in a delayed dissolution due 733  
682 to the proteins coating [115]. Moreover, Levak et al., and 734  
683 Martin et al. demonstrate a minor release of Ag<sup>+</sup> ions by 735  
684 silver nanoparticles when coated with proteins [116, 117]. 736  
685 On the other hand, the bio-molecular corona modifies 737  
686 the surface charge, but does not completely inhibit the 738  
687 surface reactivity of CNPs and FNPs, suggesting that the 739  
688 surface of the particles is still partially exposed to the sol- 740  
689 vent, and can interact directly with the cells. This effect is 741  
690 clearly dependent on the nature of the materials. Indeed, 742  
691 we have previously reported that in the case of TiO<sub>2</sub> the 743  
692 treatment with the SHDS completely inhibited the sur- 744  
693 face reactivity [39]. These results underline the impor- 745  
694 tance of the presence of active components in SHDS to 746  
695 accurately describe the NBMs transformation. 747

#### 696 **Effect of the biotransformation on the toxicity of NBMs** 697 **toward intestinal cells**

698 The pre-treatment with the SHDS largely affected the 750  
699 behaviour of NBMs toward Caco-2 cells. However, the 751  
700 effects were different, depending on the type of NBMs 752  
701 and on the model/endpoint. The treatment increased the 753  
702 toxicity of LSNPs toward undifferentiated Caco-2 cells, 754  
703 likely because of the degradation of the outermost layers' 755  
704 and the release of the surfactants, induced by the SHDS. 756  
705 On the contrary, the SHDS did not change the cytotox- 757  
706 icity of CNPs, and reduced the cytotoxicity of FNPs 758  
707 and HNPs (Fig. 8). The trend was different in primary 759  
708 epithelial intestinal cells. In this case, SHDS increased 760  
709 the toxicity of CNPs and FNPs, while LSNPs and HNPs 761  
710 maintained a toxicity trend like those observed in Caco-2 762  
711 cells (Fig. 9). Overall, the primary cells appeared to be 763  
712 more sensitive to homeostatic perturbations. This finding 764  
713 is in line with other non-transformed cell lines as CCD- 765  
714 841, which showed a stronger decrease in viability after 766  
715 treatment with isothiocyanate-capped silicon nanopar- 767  
716 ticles in comparison with Caco-2 cells [118]. Our results 768  
717 suggest that the use of primary epithelial cells helps in 769  
718 obtaining a more complete picture of the effects of NBMs 770  
719 in humans, integrating the results obtained on immortal- 771  
720 ized cells, useful for preliminary and large-scale screen- 772  
721 ings, with the results obtained in a model closer to the 773  
722 cells of the human GI tract. However, we recommend to

use both these models in parallel, in order to obtain mul-  
tiple information at the same time: if on the one hand,  
primary cells gives more reliable information on the tox-  
icity outcome in non-transformed gastro-intestinal tis-  
sue, on the other hand the use of immortalised cells that  
can form a competent gastrointestinal barrier allows to  
obtain information about the impact of NBMs on the  
barrier integrity.

Interestingly, both treated and untreated NBMs were  
not cytotoxic in the differentiated Caco-2 cells and did  
not alter the permeability of the intestinal barrier, while a  
clear perturbation of the TJs was observed for all NBMs.  
This may be interpreted as a compensatory mechanism:  
to limit the damage induced by NBMs, GI cells likely  
respond by increasing the expression of specific genes  
encoding for the main TJs proteins. By increasing the  
amount of TJs complexes, this response maintains the  
GI barrier intact, as it occurs as a compensatory mecha-  
nism in different diseases [119] or in response to IL-10,  
a cytokine increased by NBMs in our model and known  
to preserve the GI barrier integrity [29]. Indeed, while  
the pro-inflammatory cytokines TNF- $\alpha$  and IL-6, whose  
genes also are up-regulated by NBMs, are known to pro-  
mote the disruption of the GI barrier [29], also IL-10 is  
concurrently over-expressed after the exposure to NBMs:  
this balance may promote the recovery of the barrier  
integrity after an initial inflammation-related damage.  
The induction of TJ protein genes was much more evi-  
dent in SHDS-treated samples. This might be due to the  
presence of proteases derived from the SHDS in the hard  
corona, as demonstrated for FNPs. In fact, protease/anti-  
protease balance has been reported to be important in  
maintaining and regulating the intestinal permeability  
[120]. On the other hand, this effect could be compen-  
sated by the high presence of protease inhibitors derived  
from the cell media. This hypothesis should not neces-  
sarily apply to the other NBMs tested, since the protein  
corona composition is dependent on the chemical nature  
of the NBM. Conversely, it has been reported that TiO<sub>2</sub>  
nanoparticles down-regulated TJs in vivo and ex vivo in  
mice, increasing paracellular permeability [121]. In some  
cases, it is the combination of NBMs as TiO<sub>2</sub> or SiO<sub>2</sub> with  
additives found in food [122] or with bacterial toxins as  
lipopolysaccharide [123] to reduce TJ, adherens junc-  
tion and gap junction proteins [123]. Since no increase  
in the permeability of Lucifer Yellow was detected in our  
experimental conditions for all the NBMs tested, we con-  
cluded that the increase in TJs genes elicited by NBMs  
was sufficient to prevent any loss of GI barrier integrity.  
Alternatively, we cannot exclude that the integrity of the  
GI barrier that we measured was the result of a com-  
plete process of barrier reparation after an initial dam-  
age: indeed, it has been documented that Caco-2 cells



776 exposed to silica nanoparticles undergo to an initial dis-  
 777 ruption of actin cytoskeleton and TJs architecture, fol-  
 778 lowed by a recovery phase of actin remodelling and TJs  
 779 reassembly [17]. We recognize that one limitation of our  
 780 work is that we studied the acute effects only. Indeed, our  
 781 main focus was the acute toxicity of NBMs, because the  
 782 NBMs studied are used for medical purposes. Therefore,  
 783 the exposure to the gastrointestinal cells is acute and not  
 784 chronic. As follow up, we plan to monitor the TJ changes  
 785 over time, in order to have a deeper insight into the time-  
 786 dependent modulation of these parameters, focusing on  
 787 NBMs whose exposure is chronic for environmental or  
 788 occupational reasons.

789 As expected, both untreated and treated FNPs and  
 790 CNPs did not cross the barrier by transcellular or para-  
 791 cellular routes.

792 Since NBMs are not-self components it has been  
 793 widely reported that the exposure of GI barrier to NBMs  
 794 induces local inflammation, supported by the presence  
 795 of abundant lymphoid tissues associated with the intesti-  
 796 nal mucosa [124] and/or by alterations in the gut micro-  
 797 biota [125]. Also, epithelial cells physiologically produce  
 798 cytokines and chemokines that are critical in control-  
 799 ling the immune cells activation and the homeostasis  
 800 of microbiota [126]. An altered production of cytokines  
 801 from epithelial cells may result in dysbiosis, pathogenic  
 802 infections or inflammatory bowel disease [126]. As final  
 803 parameter of biocompatibility, we thus evaluated how the  
 804 NBMs tested may alter the production of pro-inflamma-  
 805 tory and anti-inflammatory cytokines by Caco-2 cells.  
 806 The increase expression in typical pro-inflammatory  
 807 cytokines as TNF and IL6, but also in anti-inflamma-  
 808 tory cytokines as IL10 and in IL22, related to GI epi-  
 809 thelial regeneration, elicited by NBMs may suggest the  
 810 development of inflammatory events induced by NBMs  
 811 exposure, paralleled by a compensatory secretion of  
 812 anti-inflammatory and pro-regenerative cytokines. This  
 813 balance, together with the over-expression of TJ genes,  
 814 likely contributes to prevent barrier damage and integ-  
 815 rity loss. Our data are in line with the work of Colombo  
 816 and co-workers, reporting that commercial ZnO nano-  
 817 particles increase IL-6 and IL-8 production in Caco-2  
 818 barrier model, maintaining barrier integrity [127]. Simi-  
 819 larly, polyvinyl chloride particles have been reported to  
 820 induce IL-1 $\beta$  secretion without altering Caco-2/HT29-  
 821 MTX/THP1 barrier integrity and viability [128]. All these  
 822 works, however, do not consider the transformation that  
 823 occurs during the NBM digestion. Indeed, in the case  
 824 of SHDS-treated NBMs, we observed a significantly  
 825 stronger increase of TJ and cytokine genes, likely because  
 826 of the dramatic modifications experienced by the NBMs  
 827 following the treatment with the SHDS. However, the  
 828 lack of increased permeability in Caco-2 barrier exposed

829 to SHDS-treated NBMs indicates that these modifica-  
 830 tions are coupled with preserved barrier integrity. Nota-  
 831 bly, CNPs had the lower effects on TJs and cytokines  
 832 genes even after digestion, confirming themselves as the  
 833 NBMs less modified during GI transit and more biocom-  
 834 patible after oral ingestion.

## 835 Conclusions

836 In this work we developed a robust and consolidated  
 837 pipeline that combines deep chemical-physical charac-  
 838 terization techniques, microscopic analysis, simulated  
 839 digestion and read-out of biological events, including  
 840 biological assays on primary cells, to provide information  
 841 on the toxicity in non-transformed gastro-intestinal tis-  
 842 sue, and on barrier-forming immortalized cells, to obtain  
 843 information about gastrointestinal barrier integrity and  
 844 inflammatory events, after acute exposure to NBMs.  
 845 Overall, the results add a piece of evidence on the impor-  
 846 tance of associating validated chemical and microscopic  
 847 characterization, SHDS methods and in vitro models  
 848 for the assessment of NBM intestinal acute toxicity and  
 849 biocompatibility. Our pipeline is versatile, meaning that  
 850 it can be applied to different NBMs that can be ingested  
 851 accidentally, for environmental or occupational reasons.  
 852 At the same time, it could provide a huge amount of  
 853 information on NBMs transformation and acute effects  
 854 on gastrointestinal tract cells. Further studies will be nec-  
 855 essary to validate the reported results in vivo.

## 856 Materials and methods

### 857 Materials and reagents

858 Plasticware for cell cultures was from Falcon (Becton  
 859 Dickinson, Franklin Lakes, NJ). FBS and culture medium  
 860 were from Invitrogen Life Technologies (Carlsbad, CA).  
 861 If not otherwise specified, reagents were purchased from  
 862 Sigma-Merck.

### 863 Nano-biomaterials (NBMs)

864 CNPs were synthesized by hydrothermal carbonization  
 865 of glucose, following a protocol previously described  
 866 [129]. CNPs are composed of elemental carbon, mainly  
 867 amorphous, and are produced as colloidal suspension in  
 868 water.

869 LSNPs, developed by Nanovector srl, Torino, Italy, are  
 870 composed by water (Citrate/Phosphate buffer pH 5), glycerol,  
 871 soy lecithin, glyceryl citrate/lactate/oleate/linoleate  
 872 (E-472), glycerol monostearate (E-471), polysorbate 20,  
 873 ascorbyl palmitate, sodium benzoate,  $\alpha$ -tocopheryl ace-  
 874 tate, strawberry flavour, sucralose and loaded with Mel-  
 875 atonin (0.1% (w/w)). FNPs are a colloidal suspension in  
 876 phosphate buffer (1 mM) of Fe<sub>3</sub>O<sub>4</sub> nanoparticles embed-  
 877 ded in a polymeric matrix (poly-lactic-co-glycolic acid/



878 polyethylene glycol) developed by Colorobbia Consult-  
879 ing, Vinci, Italy.

880 HNPs have been purchased by Sigma Aldrich (Merck  
881 KGaA, Darmstadt, Germany) in the form of a powder  
882 made of pure hydroxyapatite with stoichiometric compo-  
883 sition ( $\text{Ca}_5(\text{PO}_4)_3\text{OH}$ ).

#### 884 Dynamic light scattering (DLS)

885 Size distribution and polydispersity index (PDI) were  
886 measured on SHDS-treated and untreated NBMs diluted  
887 in ultrapure water (100  $\mu\text{g}/\text{ml}$ ) or in cell medium (DMEM  
888 supplemented with 10% FBS, 1% penicillin/streptomycin  
889 solution) (100  $\mu\text{g}/\text{ml}$ ). Measurements were performed by  
890 using the Zetasizer, Nano instrument (Malvern Instru-  
891 ments, Malvern, UK) with a 633 nm HeNe laser. Instru-  
892 ment settings were: replicate 3, equilibrium time 60 s,  
893  $T=25^\circ\text{C}$ , dispersant refractive index 1.330 (water)  
894 and 1.345 (cell medium), dispersant viscosity 0.8872 cP  
895 (water) and 0.8000 cP (cell medium), material refractive  
896 index 1.410 (LSNPs), 2.420 (CNPs), 2.420 (FNPs) and  
897 1.650 (HNPs), material absorption 1.000.

898 Untreated CNPs, LSNPs and FNPs were diluted in  
899 ultrapure water before the analysis, while HNPs were sus-  
900 pended in ultrapure water and sonicated for 5 min with a  
901 probe sonicator (Sonoplus HD3100 Bandelin, Microtip  
902 MS73, diameter 3 mm, power 100 W, amplitude 30%).  
903 SHDS-treated NBMs were analysed in the fluids without  
904 dilution. In each experiment three subsequent measure-  
905 ments were performed on the same suspension. The data  
906 were expressed as the mean of three independent experi-  
907 ments,  $\pm$  standard deviation. Each line represents the  
908 mean values of 15 measurements that were obtained in  
909 three independent experiments.

#### 910 Electrophoretic light scattering (ELS)

911  $\zeta$ -potential was measured using an electrophoretic light  
912 scattering analyzer (Zetasizer, Nano ZS Malvern Instru-  
913 ments, Malvern, UK). For  $\zeta$ -potential curve versus pH,  
914 NBMs were diluted at 500  $\mu\text{g}/\text{ml}$  in ultrapure water and  
915 pH was modified by adding NaOH 0.1 M or HCl 0.1 M.  
916 Instrument settings were: dispersant (water) dielectric  
917 constant: 78.5.

#### 918 Flow particle imaging analysis (FPIA)

919 FPIA was performed by using a Sysmex FPIA3000 ana-  
920 lyser. High power field ( $2 \times$  secondary lens) was applied,  
921 which allows measuring particles from 1 to 40  $\mu\text{m}$ . The  
922 suspensions of nanoparticles in simulated digestive fluids  
923 were centrifuged at 8000 rpm for 10 min by Rotina 380 R  
924 (Hettich Zentrifuger). The suspensions were pelleted, the  
925 supernatant was removed, and the resulting pellets were  
926 resuspended in ultrapure water for 2 min in an ultrasonic

bath. The washing process was repeated three times and  
927 5 ml of the suspensions were analysed. 928

#### Surface reactivity

929 The NBM surface reactivity was monitored by EPR  
930 analysis (Miniscope 100 EPR spectrometer, Magnettech,  
931 Berlin, Germany) using TEMPONE-H (1-hydroxy-  
932 2,2,6,6-tetramethyl-4-oxo-piperidine, Enzo Life Sciences,  
933 Inc.) as spin probe. Suspension of untreated or SHDS-  
934 treated NBMs in ultrapure water or cell medium (0.5 mg/  
935 ml) was diluted 1:1 in a 100  $\mu\text{M}$  solution of Tempone-H  
936 and the suspension constantly stirred in a glass vial. The  
937 EPR spectra were recorded on a sample aliquot (50  $\mu\text{l}$ ).  
938 Instrument settings: microwave power 7 mW, modula-  
939 tion amplitude 1 G, scan time 80 s, two scans. 940

#### Transmission electron microscope (TEM) measurements

941 TEM was accomplished utilizing a FEI CM20 microscope  
942 operating at 200 kV. TEM samples were prepared by  
943 placing one drop of a diluted sample on a carbon-coated  
944 Cu grid and allowing the solvent to evaporate. 945

#### Protein corona analysis

946 NBMs were treated with SHDS following the proto-  
947 col explained below. Treated and untreated NBMs were  
948 incubated for 24 h in DMEM 10% FBS, 1% penicillin/  
949 streptomycin at  $37^\circ\text{C}$  under agitation (0.5 mg/ml). After  
950 the incubation, the NBM-corona complex was isolated  
951 through three centrifugation/dispersion cycles in PBS.  
952 For FNPs, ferromagnetic spheres were used to isolate  
953 the complex NBMs-corona (unpublished data). For  
954 SDS-PAGE, the pellets obtained after the washing were  
955 stripped using a loading buffer (Cell Signalling Technol-  
956 ogy) in 0.1 M dithiothreitol and heated at  $100^\circ\text{C}$ . The  
957 obtained solutions were centrifuged before loading the  
958 samples in a 10% acrylamide gel. SDS-PAGE was car-  
959 ried out using the Mini-Protean (BioRad) system at 120 V  
960 until the dye front reached the end of the gel. The gels  
961 were stained using Coomassie (Thermo Scientific) and  
962 scanned with the Amersham Gel doc system. 963

964 For the mass spectrometry analysis, the samples in-  
965 gel were digested with trypsin and treated with differ-  
966 ent solutions to extract the peptides from the gel matrix.  
967 Raw mass spectrometry data were processed using the  
968 MaxQuant version 2.0.1.0. [130]. The identification of  
969 peptides and proteins was done using the UniProt data-  
970 base. Perseus software version 1.6.15.0 [131] allowed the  
971 analysis of the LFQ intensities obtained. Data were log  
972 transformed and missing values were replaced with val-  
973 ues from a normal distribution.



974 **Cell cultures**  
 975 Caco-2 epithelial colon cells were obtained from Ameri-  
 976 can Tissue Culture Collection (ATCC) and were grown  
 977 in DMEM supplemented with 20% FBS, 1% penicil-  
 978 lin/streptomycin. For the experiments, cells were used  
 979 between passage 33 and 47, and incubated in DMEM  
 980 supplemented with 10% FBS, 1% penicillin/streptomycin.  
 981 To obtain Caco-2 monolayer forming a competent intes-  
 982 tinal barrier model, cells were grown on Millicell®-96 cell  
 983 culture inserts (Merck KGaA, Darmstadt, Germany) for  
 984 21 days [132].

985 HCT116 cells were obtained from the European Col-  
 986 lection of Authenticated Cell Cultures (ECACC, cata-  
 987 logue No. #91,091,005) and were grown and exposed  
 988 to NBMs in McCoy's 5a medium containing 2 mM glu-  
 989 tamine, 10% FBS and 1% penicillin/streptomycin. Cells  
 990 were used between passage 15 and 25.

991 Human colonic epithelial cells (HCoEpiC) were pur-  
 992 chased from CliniSciences (CliniSciences, Guidonia  
 993 Montecelio, Italy) and were cultured in Colonic Epithe-  
 994 lial Cell Medium (HCoEpiCM) supplemented with 10%  
 995 (v/v) Colonic Epithelial Cell Growth Supplement  
 996 (HCoEpiCGS) and 1% penicillin/streptomycin. Experi-  
 997 ments were performed between the passage 5 and 8.

998 **Preparation of simulated digestive fluids**

999 Simulated digestive fluids were prepared following the  
 1000 protocol used by Sohal et al. [50]. The composition of  
 1001 each simulated digestive fluid is summarized in Table 4.  
 1002 For each fluid, the organic and inorganic parts were pre-  
 1003 pared separately by adding the components to ultrapure  
 1004 water and dissolving them under magnetic stirring. Then,

the two solutions were mixed in a ratio of 1:1 (v/v) and  
 stirred overnight.

The active components were added just before per-  
 forming the experiment and the solution was vortexed to  
 suspend them.

1010 **Simulated human digestion system**

1011 The protocol used for the simulated human digestion sys-  
 1012 tem (SHDS) is that used by Sohal et al. [50].

1013 A NBM suspension at the concentration of 1 mg/ml  
 1014 was SHDS-treated using an equal volume of simulated  
 1015 digestive fluids (Additional file 1: Fig S10). First, the SSF  
 1016 was added and the sample was incubated for 15 min at  
 1017 37 °C under shaking. After this time, SGF was added  
 1018 and incubated for 4 h. Finally, SIF, composed of simu-  
 1019 lated duodenal fluid (SDF) and simulated bile fluid (SBF)  
 1020 in a ratio of 2:1 (v/v), was added and incubated for fur-  
 1021 ther 4 h. The ratio of simulated digestive fluids was 1:2:3  
 1022 (Additional file 1: Fig S10). Table 4 summarises the simu-  
 1023 lated digestive fluids composition. At the end of the pro-  
 1024 cess, if necessary, pH was adjusted in the range of 6.5 and  
 1025 7.5 using 1 M NaHCO<sub>3</sub> and the suspension was sterilized  
 1026 15 min under UV radiations.

1027 For surface reactivity evaluation the suspension was  
 1028 centrifuged at 11,000 rpm (Rotina 380 R, Hettich Zentri-  
 1029 fuger) and, after discarding the supernatant, it was resus-  
 1030 pended in cell culture medium in a volume depending on  
 1031 the desired concentration.

1032 For other tests the suspension was mixed with cell  
 1033 medium to obtain the final concentration. Incubation  
 1034 with cells or intestinal barrier model was performed for  
 1035 24 h.

**Table 4** Composition of simulated digestive fluids for the SHDS model (amounts based on 100 ml of fluid)

Fluids	Saliva	Gastric juice	Duodenal fluid	Bile
pH	6.5 ± 0.1	1.4 ± 0.1	8.1 ± 0.1	8.0 ± 0.1
Inorganic fraction	89.6 mg KCl 20 mg KSCN 102.2 mg NaH <sub>2</sub> PO <sub>4</sub> ·xH <sub>2</sub> O 57 mg Na <sub>2</sub> SO <sub>4</sub> 29.8 mg NaCl Milli-Q water	30.6 mg NH <sub>4</sub> Cl 40 mg CaCl <sub>2</sub> × 2H <sub>2</sub> O 82.4 mg KCl 275.2 mg NaCl 30.6 mg NaH <sub>2</sub> PO <sub>4</sub> ·xH <sub>2</sub> O Milli-Q water	5 mg MgCl <sub>2</sub> × 6H <sub>2</sub> O 56.4 mg KCl 8 mg KH <sub>2</sub> PO <sub>4</sub> 338.8 mg NaHCO <sub>3</sub> 701.2 mg NaCl Milli-Q water	37.6 mg KCl 578.5 mg NaHCO <sub>3</sub> 525.9 mg NaCl Milli-Q water
Organic fraction	20 mg urea Milli-Q water	8.5 mg urea 65 mg D-glucose 2 mg glucuronic acid 33 mg D-glucosamine hydrochloride Milli-Q water	25 mg urea Milli-Q water	10 mg urea Milli-Q water
Active components	5 mg mucin (porcine stomach) 1.6 mg uric acid 14.5 mg α-amylase (Bacillus subtilis)	300 mg mucin (porcine stomach) 100 mg albumin (bovine serum) 100 mg pepsin (porcine gastric mucosa)	300 mg pancreatin (porcine pancreas) 50 mg lipase from (Candida rugosa) 100 mg albumin (bovine serum)	600 mg bile (bovine) 180 mg albumin (bovine serum)

1036	<b>Viability assay</b>	1085
1037	WST-1 assay, based on the cleavage of the slightly red	1086
1038	tetrazolium salt WST-1 (4-[3-(4-iodophenyl)-2-(4-	1087
1039	nitrophenyl)-2H-5-tetrazolio]-1,3-benzene disulfonate)	1088
1040	to form a dark red formazan dye by metabolically active	1089
1041	cells, was used to evaluate the cell viability, as index of	1090
1042	mitochondrial activity, after the treatment with NBMs.	1091
1043	WST-1 was added at 10% (v/v) of cell medium and the	1092
1044	absorbance was read at 440 nm after 2 h for Caco-2	1093
1045	cells, 1 h and 30 min for HCT116 cells, 4 h for HCoEpiC	1094
1046	cells and 30 min for the intestinal barrier model using a	1095
1047	Synergy HT Multi-Detection Microplate Reader (Bio-	1096
1048	Tek Instruments, Winooski, VT) or a Spectramax ID3	1097
1049	plate reader (Molecular Devices, for HCT116 cells	1098
1050	only). The absorbance value at the reference wavelength	1099
1051	(630 nm) was subtracted.	1100
1052		1101
1052	<b>Genotoxicity assay</b>	1102
1053	Genotoxicity was assessed by counting the DNA double	1103
1054	strand break repair foci, after immunostaining of	1104
1055	the 53BP1 DNA repair protein, as previously described	1105
1056	[21, 133]. Briefly, after exposure to NBMs, cells were	1106
1057	fixed with 4% paraformaldehyde, and permeabilized	1107
1058	with 0.2% v/v Triton X-100 prepared in PBS containing	1108
1059	3% w/v bovine serum albumin (PBS-BSA). Non-specific	1109
1060	sites were blocked with PBS-BSA, then incubated	1110
1061	for 1 h with rabbit polyclonal anti-TP53BP1 antibody	1111
1062	(Abnova, reference PAB12506) diluted in PBS-BSA,	1112
1063	washed three times for 5 min with PBS-BSA and incubated	
1064	for 1 h with an anti-rabbit IgG Atto 633 antibody	1113
1065	(Sigma-Aldrich, 41,176) diluted in PBS-BSA.	1114
1066	After three washing in PBS-BSA containing 0.2% Triton	1115
1067	X-100, the nuclei were stained with 0.3 µg/ml	1116
1068	Hoechst 33,342 (Sigma-Aldrich) for 20 min at room	1117
1069	temperature. The number of cell nuclei and the average	1118
1070	number of 53BP1 foci per cell nucleus were counted	1119
1071	using a CellInsight CX5 High-Content Screening Plat-	1120
1072	form (Thermo Fisher Scientific). This experiment was	1121
1073	repeated three times independently, with <i>n</i> = 5 repli-	1122
1074	cates in each independent experiment.	1123
1075		1124
1075	<b>Trans-Epithelial Electrical Resistance (TEER)</b>	1125
1076	To evaluate the barrier formation and integrity of Caco-2	1126
1077	barrier model after the exposure to NBMs, TEER was	1127
1078	measured using the Millicell <sup>®</sup> ERS-2 voltohmmeter	1128
1079	(Merck KGaA, Darmstadt, Germany). The resistance was	1129
1080	read in ohms and the resistivity was calculated by sub-	
1081	tracting the cell-free inserts value from the cell-contain-	1130
1082	ing inserts, multiplying for the cells growth area. Only	1131
1083	the monolayer with values >250 Ω·cm <sup>2</sup> were used for	1132
1084	exposure to NBMs.	1133
1085		
1085	<b>Evaluation of barrier permeability</b>	1130
1086	To evaluate the permeability of the intestinal barrier	1131
1087	model the trans-epithelial passage of Lucifer Yellow fluo-	1132
1088	rescent dye [134] was measured following the NANoREG	1133
1089	SOP (Standard Operating Procedure for evaluation of	
1090	NPs impact on Caco2 cell barrier model). After collec-	
1091	tion of the medium, the cells and the basolateral com-	
1092	partment of Millicell <sup>®</sup> -96 cell culture inserts were rinsed	
1093	thrice with Hanks' Balanced Salt Solution (HBSS). Then	
1094	50 µl/well of a 0.4 mg/ml Lucifer Yellow solution in HBSS	
1095	were added in the apical compartment. After 2 h of incu-	
1096	bation at 37 °C, the apparent permeability (Papp) and	
1097	the percentage of fluorophore recovered from the lower	
1098	chamber in cell-free inserts were calculated, reading the	
1099	relative fluorescence units (RFUs) (λ excitation: 504 nm,	
1100	λ emission: 529 nm), with a Synergy HT Multi-Detection	
1101	Microplate Reader.	
1102		
1102	<b>NBMs absorption through the intestinal barrier</b>	1102
1103	<b>by Nanoparticle Tracking Analysis (NTA)</b>	1103
1104	The CNPs and FNPs passage through the Caco-2 intes-	1104
1105	tinal barrier was evaluated by measuring the number of	1105
1106	particles in the initial suspension and in the basolateral	1106
1107	compartment of the Millicell <sup>®</sup> -96 cell culture inserts	1107
1108	using Nanoparticle Tracking Analysis (NTA, ZetaView,	1108
1109	Particle Metrix GmbH, Germany). The samples were	1109
1110	diluted in ultrapure water before the analysis. Sensitivity	1110
1111	was set at 60 and shutter value at 100. In this condition	1111
1112	neither phenol red nor FBS interference was detected.	1112
1113		
1113	<b>FNPs absorption through the intestinal barrier</b>	1113
1114	<b>by colorimetric assay</b>	1114
1115	For the quantification of FNPs in the basolateral com-	1115
1116	partment the FerroZine <sup>™</sup> -based colorimetric assay was	1116
1117	used based on the protocols reported by Balivada and co-	1117
1118	workers [135] and by Jeinter [136]. First, to dissolve and	1118
1119	reduce the iron contained in FNPs, 150 µl of the samples	1119
1120	were incubated at 70 °C for 2 h with 150 µl of 1.2 M HCl	1120
1121	and 60 µl of 1 M ascorbic acid. Then, 300 µl of the result-	1121
1122	ing solution were incubated with 200 µl of 1.5 M sodium	1122
1123	acetate, 50 µl of 1 M ascorbic acid, 350 µl of ultrapure	1123
1124	water, and 100 µl of 21 mM FerroZine <sup>™</sup> (Thermo Fisher	1124
1125	Scientific). After 20 min of incubation at room tem-	1125
1126	perature, the absorbance at 562 nm was measured by	1126
1127	an UV-Vis spectrophotometer (UVICON 930, Kontron	1127
1128	Instruments, Basel, Switzerland) and the concentration	1128
1129	was calculated using a calibration curve.	1129
1130		
1130	<b>Quantitative Real-Time PCR (qRT-PCR)</b>	1130
1131	mRNA was extracted using the phenol/chloroform/	1131
1132	ethanol method: cells were lysed in 0.5 ml RiboZol	1132
1133	(VWR; Radnor, PA) and incubated for 10 min at room	1133



1134 temperature, and then 0.2 ml chloroform was added.  
 1135 Samples were shaken for 15 s and incubated at room  
 1136 temperature for 3 min before being centrifuged for  
 1137 15 min at 12,000g at 4 °C. Aqueous phase was trans-  
 1138 ferred in a new tube and 0.2 ml isopropanol was added,  
 1139 the samples were incubated for 10 min at room tem-  
 1140 perature before centrifugation at 12,000g for 10 min at  
 1141 4 °C. RNA pellets were washed twice with ethanol 70%  
 1142 v/v by centrifuging at 12,000g for 5 min at 4 °C, and  
 1143 were resuspended in RNase-free water. The RNA quan-  
 1144 tification was performed using the Take3 plate (Syn-  
 1145 ergy HT Multi-Detection Microplate Reader), reading  
 1146 the absorbance at 260 nm. The reverse transcription of  
 1147 RNA samples was performed using the iScript cDNA  
 1148 synthesis kit (Bio-Rad, Segrate, Italy), according to the  
 1149 manufacturer’s instructions.

1150 To quantify the expression of CLDN3, CLDN5,  
 1151 OCLN, TJP1, IL-6, IL-10, IL-22 and TNF-α, qRT-PCR  
 1152 was carried out using as gene reference the ribosomal  
 1153 protein unit S14 coding gene. Briefly, 5 µl of iTaq Uni-  
 1154 versal SYBR Green Supermix (Bio-Rad Laboratories),  
 1155 2 µl of 5 µM primers mix (Table 5) and 3 µl of cDNA  
 1156 (5 ng/µl) were used for each sample. Samples were run  
 1157 using a CFX96 Real-Time System (Bio-Rad Laborato-  
 1158 ries) for 30 s at 95 °C, 5 s at 95 °C and 30 s at 60 °C for  
 1159 42 cycles. The analysis was performed using Bio-Rad  
 1160 CFX Maestro software (Bio-Rad Laboratories).

1161 **Statistical analysis**

1162 Statistics were performed using ANOVA (ANalysis  
 1163 Of VAriance) with post-hoc Tukey Honestly Signifi-  
 1164 cant Difference Test Calculator for comparing multiple  
 1165 treatments [137], using Statistical Package for Social  
 1166 Science software (IBM SPSS Statistics v.19). *p* < 0.05  
 1167 was considered significant.  
 1168

**Table 5** Sequences of qRT-PCR primers

Gene	Forward (5’-3’)	Reverse (5’-3’)
TJP1	CCCCACTCTGAAAATGAGGA	ACAGCAATGGAGGAAACAGC
OCLN	ATGCCATGGGACTGTCAACT	TTTGTGGGACAAGGAACACA
CLDN3	CCTGCGTCTGTCCCTTAGAC	CACGCGAGAAGAAGTACACG
CLDN5	GCTGTTCCATAGGCAGAGC	CCCTGCCATGGAGTAAAGA
TNF	TGGGATCATTGCCCTGTGAG	GGTGCTGAAGGAGGGGTA
IL6	GGTACATCCTCGACGGCATCT	GTGCCTCTTGTGCTTTTAC
IL10	AGACAGACTGCAAAGAAGGC	TCAAGCATGTTAGGCAGGTT
IL22	GCTGCCTCCTTCTTGG	GTGCGGTTGGTATAGG
S14	AGGTGCAAGGAGCTGGTT	TCCAGGGTCTTGGTCTATT

**Abbreviations**

53BP1: Tumour Suppressor P53-binding Protein 1; ANOVA: ANalysis Of  
 VAriance; BSA: Bovine serum albumin; CLDN: Claudin encoding gene; CNPs:  
 Carbon nanoparticles; d<sub>h</sub>: Hydrodynamic diameter; DLS: Dynamic light  
 scattering; DMEM: Dulbecco’s modified eagle medium; ELS: Electrophoretic  
 light scattering; EPR: Electron paramagnetic resonance spectroscopy; FBS:  
 Foetal bovine serum; FNPs: Magnetite nanoparticles; FPIA: Flow particle  
 imaging analysis; GI: Gastro-intestinal; HBSS: Hanks’ Balanced Salt Solution;  
 HNPs: Hydroxyapatite nanoparticles; Ig: Immunoglobulin; IL: Interleukin; LFO:  
 Label free quantification; LSNPs: Lipid surfactant nanoparticles; NBM: Nano-  
 biomaterial; NTA: Nanoparticle tracking analysis; OCLN: Occludin encoding  
 gene; OGI: Oral-gastro-intestinal; Papp: Apparent permeability; PBS: Phosphate  
 buffered saline; PDI: Polydispersity index; PEG: Poly(Ethylene glycol); PLGA:  
 Poly(lactic-co-glycolic acid); qRT-PCR: Quantitative Real Time-Polymerase  
 Chain Reaction; RFU: Relative fluorescence units; SBF: Simulated bile fluid; SD:  
 Standard deviation; SDF: Simulated duodenal fluid; SDS-PAGE: Sodium Dode-  
 cyl Sulphate-PolyAcrylamide Gel Electrophoresis; SEM: Standard error of the  
 mean; SGF: Simulated gastric fluid; SHDS: Simulated human digestion system;  
 SIF: Simulated intestinal fluid; SSF: Simulated saliva fluid; TEM: Transmission  
 electron microscope; TJs: Tight junctions; TNF: Tumour necrosis factor; TJP:  
 Zonula Occludens encoding gene.

**Supplementary Information**

The online version contains supplementary material available at <https://doi.org/10.1186/s12989-022-00491-w>.

**Additional file 1.**

**Acknowledgements**

The Authors thank Mr. Costanzo Costamagna, Department of Oncology,  
 University of Torino, for the technical assistance and Dr. Marta Vassallo for her  
 contribution in some investigations.

**Author contributions**

Conceptualization, CR, IF and EB; methodology, AM, EG, FB, PG, MM, and MC;  
 investigation, GA, PK, EPG, GB, CR, AG-P, SS, MGS, DB; data curation, GA, MC,  
 MM, CR, IF; writing—original draft preparation GA, EPG; writing—review and  
 editing, CR, IF, EB, PG, MM, MC and CC; funding acquisition, IF, EB, MC, CC,  
 and MM. All authors have read and agreed to the published version of the  
 manuscript.

**Funding**

This research has received funding by the European Union’s Horizon 2020,  
 Research and Innovation Program “BIORIMA”, under Grant Agreement No.  
 760928.

**Availability of data and materials**

All data generated or analysed during this study are included in this published  
 article and its additional files.

**Declarations**

**Ethics approval and consent to participate**

Not applicable.

**Consent for publication**

Not applicable.

**Competing interests**

The authors declare that they have no competing interests.

**Author details**

<sup>1</sup>Department of Chemistry, University of Turin, Via Pietro Giuria 7, 10125 Turin,  
 Italy. <sup>2</sup>Department of Public Health and Pediatrics, University of Turin, Piazza  
 Polonia, 94, 10126 Turin, Italy. <sup>3</sup>Department of Oncology, University of Turin,  
 Via Santena 5 bis, 10126 Turin, Italy. <sup>4</sup>Department of Life Sciences and Systems  
 Biology, University of Turin, Via Accademia Albertina 13, 10123 Turin, Italy.  
<sup>5</sup>Research Unit of Advanced, Composite, Nano-Materials and Nanotechnology,



1226 School of Chemical Engineering, National Technical University of Athens,  
 1227 9 Heron Polytechniou St., 15780 Zographos, Athens, Greece. <sup>6</sup>Colorobbia  
 1228 Consulting Srl, Headwork, Via Pietramarina, 53, 50059 Sovigliana, Vinci, FI,  
 1229 Italy. <sup>7</sup>Nanovector Srl, Headwork, Via Livorno 60, 10144 Turin, Italy. <sup>8</sup>National  
 1230 Research Council, Institute of Science and Technology for Ceramics ISTECCNR,  
 1231 Via Granarolo 64, 48018 Faenza, RA, Italy. <sup>9</sup>Department of Chemistry, Royal  
 1232 College of Surgeons in Ireland (RCSI), 123 St Stephen Green, Dublin 2, Ireland.  
 1233 <sup>10</sup>CEA, NIRG, SyMMES-CIBEST, Université Grenoble Alpes, 38000 Greno-  
 1234 ble, France.

Received: 9 February 2022 Accepted: 29 June 2022

1235  
1236

References

1237  
1238  
1239  
1240  
1241  
1242  
1243  
1244  
1245  
1246  
1247  
1248  
1249  
1250  
1251  
1252  
1253  
1254  
1255  
1256  
1257  
1258  
1259  
1260  
1261  
1262  
1263  
1264  
1265  
1266  
1267  
1268  
1269  
1270  
1271  
1272  
1273  
1274  
1275  
1276  
1277  
1278  
1279  
1280  
1281  
1282  
1283  
1284  
1285  
1286  
1287  
1288  
1289  
1290

1. Conte A, Longano D, Costa C, Ditaranto N, Ancona A, Cioffi N, et al. A novel preservation technique applied to fiordilatte cheese. *Innov Food Sci Emerg Technol*. 2013;19:158–65.
2. da Costa BS, Bresolin JD, Sivieri K, Ferreira MD. Low-density polyethylene films incorporated with silver nanoparticles to promote antimicrobial efficiency in food packaging. *Food Sci Technol Int*. 2020;26:353–66.
3. Esfahani R, Jafari SM, Jafarpour A, Dehnad D. Loading of fish oil into nanocarriers prepared through gelatin-gum Arabic complexation. *Food Hydrocoll*. 2019;90:291–8.
4. Pulit-Prociak J, Chwastowski J, Siudek M, Banach M. Incorporation of metallic nanoparticles into cosmetic preparations and assessment of their physicochemical and utility properties. *J Surfactants Deterg*. 2018;21:575–91.
5. Jiménez-Pérez ZE, Singh P, Kim YJ, Mathiyalagan R, Kim DH, Lee MH, et al. Applications of Panax ginseng leaves-mediated gold nanoparticles in cosmetics relation to antioxidant, moisture retention, and whitening effect on B16BL6 cells. *J Ginseng Res*. 2018;42:327–33.
6. Yang X, Yang F, Walboomers XF, Bian Z, Fan M, Jansen JA. The performance of dental pulp stem cells on nanofibrous PCL/gelatin/nHA scaffolds. *J Biomed Mater Res Part A*. 2010;93A:247–57.
7. Adamiak M, Cheng G, Bobis-Wozowicz S, Zhao L, Kedracka-Krok S, Samanta A, et al. Induced pluripotent stem cell (iPSC)-derived extracellular vesicles are safer and more effective for cardiac repair than iPSCs. *Circ Res*. 2018;122:296–309.
8. González-Fernández Y, Zalacain M, Imbuluzqueta E, Sierrasesumaga L, Patiño-García A, Blanco-Prieto MJ. Lipid nanoparticles enhance the efficacy of chemotherapy in primary and metastatic human osteosarcoma cells. *J Drug Deliv Sci Technol*. 2015;30:435–42.
9. González-Fernández Y, Imbuluzqueta E, Zalacain M, Mollinedo F, Patiño-García A, Blanco-Prieto MJ. Doxorubicin and edelfosine lipid nanoparticles are effective acting synergistically against drug-resistant osteosarcoma cancer cells. *Cancer Lett*. 2017;388:262–8.
10. do Pereira AES, Oliveira HC, Fraceto LF. Polymeric nanoparticles as an alternative for application of gibberellic acid in sustainable agriculture: a field study. *Sci Rep*. 2019;9:7135.
11. Pandey K, Anas M, Hicks VK, Green MJ, Khodakovskaya MV. Improvement of commercially valuable traits of industrial crops by application of carbon-based nanomaterials. *Sci Rep*. 2019;9:19358.
12. Pietroiusti A, Bergamaschi E, Campagna M, Campagnolo L, De Palma G, Iavicoli S, et al. The unrecognized occupational relevance of the interaction between engineered nanomaterials and the gastro-intestinal tract: a consensus paper from a multidisciplinary working group. *Part Fibre Toxicol*. 2017;14:47.
13. Bouwmeester H, van der Zande M, Jepson MA. Effects of food-borne nanomaterials on gastrointestinal tissues and microbiota. *WIREs Nanomed Nanobiotechnol*. 2018;10:e1481.
14. Vermette D, Hu P, Canarie MF, Funaro M, Glover J, Pierce RW. Tight junction structure, function, and assessment in the critically ill: a systematic review. *Intensive Care Med Exp*. 2018;6:37.
15. Oshima T, Miwa H, Joh T. Changes in the expression of claudins in active ulcerative colitis. *J Gastroenterol Hepatol*. 2008;23:S146–50.
16. Zeissig S, Bürgel N, Günzel D, Richter J, Mankertz J, Wahnschaffe U, et al. Changes in expression and distribution of claudin 2, 5 and 8 lead to

discontinuous tight junctions and barrier dysfunction in active Crohn's disease. *Gut*. 2007;56:61–72.

17. Cornu R, Chrétien C, Pellequer Y, Martin H, Béduneau A. Small silica nanoparticles transiently modulate the intestinal permeability by actin cytoskeleton disruption in both Caco-2 and Caco-2/HT29-MTX models. *Arch Toxicol*. 2020;94:1191–202.
18. Ruiz PA, Morón B, Becker HM, Lang S, Atrott K, Spalinger MR, et al. Titanium dioxide nanoparticles exacerbate DSS-induced colitis: role of the NLRP3 inflammasome. *Gut*. 2017;66:1216–24.
19. Sohal IS, O'Fallon KS, Gaines P, Demokritou P, Bello D. Ingested engineered nanomaterials: state of science in nanotoxicity testing and future research needs. *Part Fibre Toxicol*. 2018;15:29.
20. Farcas L, Torres Andón F, Di Cristo L, Rotoli BM, Bussolati O, Bergamaschi E, et al. Comprehensive in vitro toxicity testing of a panel of representative oxide nanomaterials: first steps towards an intelligent testing strategy. *PLoS ONE*. 2015;10:e0127174.
21. Dorier M, Tisseyre C, Dussert F, Béal D, Arnal ME, Douki T, et al. Toxicological impact of acute exposure to E171 food additive and TiO2 nanoparticles on a co-culture of Caco-2 and HT29-MTX intestinal cells. *Mutat Res Toxicol Environ Mutagen*. 2019;845:402980.
22. Dorier M, Béal D, Tisseyre C, Marie-Desvergne C, Dubosson M, Barreau F, et al. The food additive E171 and titanium dioxide nanoparticles indirectly alter the homeostasis of human intestinal epithelial cells in vitro. *Environ Sci Nano*. 2019;6:1549–61.
23. Dorier M, Béal D, Marie-Desvergne C, Dubosson M, Barreau F, Houdeau E, et al. Continuous in vitro exposure of intestinal epithelial cells to E171 food additive causes oxidative stress, inducing oxidation of DNA bases but no endoplasmic reticulum stress. *Nanotoxicology*. 2017;11:751–61.
24. Basak SC, Vracko M, Witzmann FA. Mathematical nanotoxicoprotoeomics: quantitative characterization of effects of multi-walled carbon nanotubes (MWCNT) and TiO2 Nanobelts (TiO2-NB) on protein expression patterns in human intestinal cells. *Curr Comput Aided Drug Des*. 2016;12:259–64.
25. Lai X, Agarwal M, Lvov YM, Pachpande C, Varahramyan K, Witzmann FA. Proteomic profiling of halloysite clay nanotube exposure in intestinal cell co-culture. *J Appl Toxicol*. 2013;33:1316–29.
26. Lai YH, D'Souza MJ. Microparticle transport in the human intestinal M cell model. *J Drug Target*. 2008;16:36–42.
27. Stagg AJ. Intestinal dendritic cells in health and gut inflammation. *Front Immunol*. 2018;9:2883.
28. Yang R, Liao Y, Wang L, He P, Hu Y, Yuan D, et al. Exosomes derived from M2b macrophages attenuate DSS-induced colitis. *Front Immunol*. 2019;10:2346.
29. Al-Sadi R, Boivin M, Ma T. Mechanism of cytokine modulation of epithelial tight junction barrier. *Front Biosci*. 2009;14:2765–78.
30. Susewind J, de Souza C-W, Repnik U, Collnot E-M, Schneider-Daum N, Griffiths GW, et al. A 3D co-culture of three human cell lines to model the inflamed intestinal mucosa for safety testing of nanomaterials. *Nanotoxicology*. 2016;10:53–62.
31. Leonard F, Ali H, Collnot E-M, Crielgaard BJ, Lammers T, Storm G, et al. Screening of budesonide nanoformulations for treatment of inflammatory bowel disease in an inflamed 3D cell-culture model. *Altx*. 2012;29:275–85.
32. Meirelles GC, Mendes C, Caon T, Teixeira HF, von Poser G, Ponchel G. Intestinal permeability enhancement of benzopyran HP1-loaded nanoemulsions. *Eur J Pharm Sci Off J Eur Fed Pharm Sci*. 2019;127:115–20.
33. Krupa L, Bajka B, Staroń R, Dupont D, Singh H, Gutkowski K, et al. Comparing the permeability of human and porcine small intestinal mucus for particle transport studies. *Sci Rep*. 2020;10:20290.
34. Tada-Oikawa S, Eguchi M, Yasuda M, Izuoka K, Ikegami A, Vranic S, et al. Functionalized surface-charged SiO(2) nanoparticles induce pro-inflammatory responses, but are not lethal to Caco-2 cells. *Chem Res Toxicol*. 2020;33:1226–36.
35. Taboada-López MV, Leal-Martínez BH, Domínguez-González R, Bermejo-Barrera P, Taboada-Antelo P, Moreda-Piñeiro A. Caco-2 in vitro model of human gastrointestinal tract for studying the absorption of titanium dioxide and silver nanoparticles from seafood. *Talanta*. 2021;233:122494.
36. Hempt C, Kaiser J-P, Scholder O, Buerki-Thurnherr T, Hofmann H, Rippl A, et al. The impact of synthetic amorphous silica (E 551) on differentiated

1291  
1292  
1293  
1294  
1295  
1296  
1297  
1298  
1299  
1300  
1301  
1302  
1303  
1304  
1305  
1306  
1307  
1308  
1309  
1310  
1311  
1312  
1313  
1314  
1315  
1316  
1317  
1318  
1319  
1320  
1321  
1322  
1323  
1324  
1325  
1326  
1327  
1328  
1329  
1330  
1331  
1332  
1333  
1334  
1335  
1336  
1337  
1338  
1339  
1340  
1341  
1342  
1343  
1344  
1345  
1346  
1347  
1348  
1349  
1350  
1351  
1352  
1353  
1354  
1355  
1356  
1357  
1358  
1359  
1360  
1361



- Caco-2 cells, a model for the human intestinal epithelium. *Toxicol In Vitro*. 2020;67:104903.
37. Bertero A, Colombo G, Cortinovic C, Bassi V, Moschini E, Bellitto N, et al. In vitro copper oxide nanoparticle toxicity on intestinal barrier. *J Appl Toxicol*. 2021;41:291–302.
38. Vecchiotti G, Colafarina S, Aloisi M, Zarivi O, Di Carlo P, Poma A. Genotoxicity and oxidative stress induction by polystyrene nanoparticles in the colorectal cancer cell line HCT116. *PLoS ONE*. 2021;16:e0255120.
39. Maruccio A, Prono M, Beal D, Alasonati E, Fisicaro P, Bergamaschi E, et al. Biotransformation of food-grade and nanometric TiO<sub>2</sub> in the oral-gastro-intestinal tract: driving forces and effect on the toxicity toward intestinal epithelial cells. *Nanomaterials*. 2020;10:2132.
40. Proquin H, Rodríguez-Ibarra C, Moonen CGJ, Urrutia Ortega IM, Briedé JJ, de Kok TM, et al. Titanium dioxide food additive (E171) induces ROS formation and genotoxicity: contribution of micro and nano-sized fractions. *Mutagenesis*. 2017;32:139–49.
41. Jia M, Zhang W, He T, Shu M, Deng J, Wang J, et al. Evaluation of the genotoxic and oxidative damage potential of silver nanoparticles in human NCM460 and HCT116 cells. *Int J Mol Sci*. 2020;21:1618.
42. Hayder M, Wojcieszek J, Asztemborska M, Zhou Y, Ruzik L. Analysis of cerium oxide and copper oxide nanoparticles bioaccessibility from radish using SP-ICP-MS. *J Sci Food Agric*. 2020;100:4950–8.
43. Shi JH, Axson JL, Bergin IL, Ault AP. Nanoparticle digestion simulator reveals pH-dependent aggregation in the gastrointestinal tract. *Anal Chem*. 2020;92:12257–64.
44. Zhou P, Guo M, Cui X. Effect of food on orally-ingested titanium dioxide and zinc oxide nanoparticle behaviors in simulated digestive tract. *Chemosphere*. 2021;268:128843.
45. Fadeel B, Feliu N, Vogt C, Abdelmonem AM, Parak WJ. Bridge over troubled waters: understanding the synthetic and biological identities of engineered nanomaterials. *WIREs Nanomed Nanobiotechnol*. 2013;5:111–29.
46. Ahmad M, Gani A. Ultrasonicated resveratrol loaded starch nanocapsules: characterization, bioactivity and release behaviour under in-vitro digestion. *Carbohydr Polym*. 2021;251:117111.
47. Liang X, Cao K, Li W, Li X, McClements DJ, Hu K. Tannic acid-fortified zein-pectin nanoparticles: stability, properties, antioxidant activity, and in vitro digestion. *Food Res Int*. 2021;145:110425.
48. DeLoid GM, Wang Y, Kapronezai K, Lorente LR, Zhang R, Pyrgiotakis G, et al. An integrated methodology for assessing the impact of food matrix and gastrointestinal effects on the biokinetics and cellular toxicity of ingested engineered nanomaterials. *Part Fibre Toxicol*. 2017;14:40.
49. Dufefoi W, Rabesona H, Rivard C, Mercier-Bonin M, Humbert B, Terrisse H, et al. In vitro digestion of food grade TiO<sub>2</sub> (E171) and TiO<sub>2</sub> nanoparticles: physicochemical characterization and impact on the activity of digestive enzymes. *Food Funct*. 2021;12:5975–88.
50. Sohal IS, Cho YK, O'Fallon KS, Gaines P, Demokritou P, Bello D. Dissolution behavior and biodegradability of ingested engineered nanomaterials in the gastrointestinal environment. *ACS Nano*. 2018;12:8115–28.
51. Setyawati MI, Zhao Z, Ng KW. Transformation of nanomaterials and its implications in gut nanotoxicology. *Small*. 2020;16:e2001246.
52. Llewellyn SV, Kämpfer A, Keller JG, Vilsmeier K, Büttner V, Ag Seleci D, et al. Simulating nanomaterial transformation in cascaded biological compartments to enhance the physiological relevance of in vitro dosing regimes: optional or required? *Small*. 2021;17:e2004630.
53. Bitounis D, Parviz D, Cao X, Amadei CA, Vecitis CD, Sunderland EM, et al. Synthesis and physicochemical transformations of size-sorted graphene oxide during simulated digestion and its toxicological assessment against an in vitro model of the human intestinal epithelium. *Small*. 2020;16:e1907640.
54. Gerloff K, Pereira DIA, Faria N, Boots AW, Kolling J, Förster I, et al. Influence of simulated gastrointestinal conditions on particle-induced cytotoxicity and interleukin-8 regulation in differentiated and undifferentiated Caco-2 cells. *Nanotoxicology*. 2013;7:353–66.
55. Cheng J, Teply BA, Jeong SY, Yim CH, Ho D, Sherifi I, et al. Magnetically responsive polymeric microparticles for oral delivery of protein drugs. *Pharm Res*. 2006;23:557–64.
56. Zhao Q, Lin Y, Han N, Li X, Geng H, Wang X, et al. Mesoporous carbon nanomaterials in drug delivery and biomedical application. *Drug Deliv*. 2017;24:94–107.
57. Zhang Y, Zhang L, Ban Q, Li J, Li C-H, Guan Y-Q. Preparation and characterization of hydroxyapatite nanoparticles carrying insulin and gallic acid for insulin oral delivery. *Nanomedicine*. 2018;14:353–64.
58. Dilnawaz F. Polymeric biomaterial and lipid based nanoparticles for oral drug delivery. *Curr Med Chem*. 2017;24:2423–38.
59. Huang Y, Qi M, Zhang M, Liu H, Yang D. Degradation mechanisms of poly (lactic-co-glycolic acid) films in vitro under static and dynamic environment. *Trans Nonferrous Met Soc China*. 2006;16:s293–7.
60. Schoepf JJ, Bi Y, Kidd J, Herckes P, Hristovski K, Westerhoff P. Detection and dissolution of needle-like hydroxyapatite nanomaterials in infant formula. *NanoImpact*. 2017;5:22–8.
61. Feeny OM, Williams HD, Pouton CW, Porter CJH. "Stealth" lipid-based formulations: poly(ethylene glycol)-mediated digestion inhibition improves oral bioavailability of a model poorly water soluble drug. *J Control Release*. 2014;192:219–27.
62. Maruccio A, Carella E, Fenoglio I. A comparative study on the efficacy of different probes to predict the photo-activity of nano-titanium dioxide toward biomolecules. *R Soc Chem*. 2015;5:8959–68.
63. Monopoli MP, Pitek AS, Lynch I, Dawson KA. Formation and characterization of the nanoparticle-protein corona. *Methods Mol Biol*. 2013;1025:137–55.
64. Zheng X, Baker H, Hancock WS, Fawaz F, McCaman M, Pungor EJ. Proteomic analysis for the assessment of different lots of fetal bovine serum as a raw material for cell culture. Part IV. Application of proteomics to the manufacture of biological drugs. *Biotechnol Prog*. 2006;22:1294–300.
65. Ferruzza S, Rossi C, Scarino ML, Sambuy Y. A protocol for in situ enzyme assays to assess the differentiation of human intestinal Caco-2 cells. *Toxicol In Vitro*. 2012;26:1247–51.
66. Peterson MD, Mooseker MS. Characterization of the enterocyte-like brush border cytoskeleton of the C2BBE clones of the human intestinal cell line, Caco-2. *J Cell Sci*. 1992;102:581–600.
67. Matsumoto T, Kaifuchi N, Mizuhara Y, Warabi E, Watanabe J. Use of a Caco-2 permeability assay to evaluate the effects of several Kampo medicines on the drug transporter P-glycoprotein. *J Nat Med*. 2018;72:897–904.
68. Shekhawat P, Bagul M, Edwankar D, Pokharkar V. Enhanced dissolution/caco-2 permeability, pharmacokinetic and pharmacodynamic performance of re-dispersible eprosartan mesylate nanopowder. *Eur J Pharm Sci Off J Eur Fed Pharm Sci*. 2019;132:72–85.
69. Ishiguro Y. Mucosal proinflammatory cytokine production correlates with endoscopic activity of ulcerative colitis. *J Gastroenterol*. 1999;34:66–74.
70. Kühn R, Löhler J, Rennick D, Rajewsky K, Müller W. Interleukin-10-deficient mice develop chronic enterocolitis. *Cell*. 1993;75:263–74.
71. Lindemans CA, Calafiore M, Mertelsmann AM, O'Connor MH, Dudakov JA, Jenq RR, et al. Interleukin-22 promotes intestinal-stem-cell-mediated epithelial regeneration. *Nature*. 2015;528:560–4.
72. Lo BC, Shin SB, Canals Hernaez D, Refaelli I, Yu HB, Goebeler V, et al. IL-22 preserves gut epithelial integrity and promotes disease remission during chronic salmonella infection. *J Immunol*. 2019;202:956–65.
73. Miller MR, Raftis JB, Langrish JP, McLean SG, Samutrtai P, Connell SP, et al. Inhaled nanoparticles accumulate at sites of vascular disease. *ACS Nano*. 2017;11:4542–52.
74. Milto IV, Ivanova VV, Shevtsova NM, Sukhodolov IV. Rat blood leukocytes after intravenous injection of chitosan-modified magnetic nanoparticles. *Bull Exp Biol Med*. 2020;168:785–8.
75. Stefaniak AB, Duling MG, Lawrence RB, Thomas TA, LeBouf RF, Wade EE, et al. Dermal exposure potential from textiles that contain silver nanoparticles. *Int J Occup Environ Health*. 2014;20:220–34.
76. Lamson NG, Berger A, Fein KC, Whitehead KA. Anionic nanoparticles enable the oral delivery of proteins by enhancing intestinal permeability. *Nat Biomed Eng*. 2020;4:84–96.
77. Xavier M, Garcia-Hevia L, Amado IR, Pastrana L, Gonçalves C. In vitro intestinal uptake and permeability of fluorescently-labelled hyaluronic acid nanogels. *Int J Nanomed*. 2019;14:9077–88.
78. de Lima IA, Khalil NM, Tominaga TT, Lechanteur A, Sarmento B, Mainardes RM. Mucoadhesive chitosan-coated PLGA nanoparticles for oral delivery of ferulic acid. *Artif Cells Nanomed Biotechnol*. 2018;46:993–1002.



- 1502 79. Tian Y, Xu J, Li Y, Zhao R, Du S, Lv C, et al. MicroRNA-31 reduces inflam-  
1503 matory signaling and promotes regeneration in colon epithelium, and  
1504 delivery of mimics in microspheres reduces colitis in mice. *Gastroenterol-  
1505 ogy*. 2019;156:2281-2296.e6.
- 1506 80. Lin Q, Liang R, Ye A, Singh H, Zhong F. Effects of calcium on  
1507 lipid digestion in nanoemulsions stabilized by modified starch:  
1508 implications for bioaccessibility of  $\beta$ -carotene. *Food Hydrocoll*.  
1509 2017;73:184-93.
- 1510 81. Bourlieu C, Ménard O, Bouzerzour K, Mandalari G, Macierzanka A,  
1511 Mackie AR, et al. Specificity of infant digestive conditions: some  
1512 clues for developing relevant in vitro models. *Crit Rev Food Sci Nutr*.  
1513 2014;54:1427-57.
- 1514 82. Abdelkhalik A, van der Zande M, Undas AK, Peters RJB, Bouwmeester  
1515 H. Impact of in vitro digestion on gastrointestinal fate and uptake of  
1516 silver nanoparticles with different surface modifications. *Nanotoxicol-  
1517 ogy*. 2020;14:111-26.
- 1518 83. Aditya NP, Macedo AS, Doktorovova S, Souto EB, Kim S, Chang P-S,  
1519 et al. Development and evaluation of lipid nanocarriers for quercetin  
1520 delivery: a comparative study of solid lipid nanoparticles (SLN),  
1521 nanostructured lipid carriers (NLC), and lipid nanoemulsions (LNE).  
1522 *LWT Food Sci Technol*. 2014;59:115-21.
- 1523 84. Nel A, Xia T, Mädler L, Li N. Toxic potential of materials at the  
1524 nanolevel. *Science*. 2006;311:622-7.
- 1525 85. Fubini B, Ghiazza M, Fenoglio I. Physico-chemical features of  
1526 engineered nanoparticles relevant to their toxicity. *Nanotoxicology*.  
1527 2010;4:347-63.
- 1528 86. Prokopovich P. Interactions between mammalian cells and nano- or  
1529 micro-sized wear particles: physico-chemical views against biological  
1530 approaches. *Adv Colloid Interface Sci*. 2014;213:36-47.
- 1531 87. Gehr P. Interaction of nanoparticles with biological systems. *Colloids  
1532 Surf B Biointerfaces*. 2018;172:395-9.
- 1533 88. Hinderliter PM, Minard KR, Orr G, Chrisler WB, Thrall BD, Pounds JG,  
1534 et al. ISDD: a computational model of particle sedimentation, diffu-  
1535 sion and target cell dosimetry for in vitro toxicity studies. *Part Fibre  
1536 Toxicol*. 2010;7:36.
- 1537 89. Marucco A, Aldieri E, Leinardi R, Bergamaschi E, Riganti C, Fenoglio I.  
1538 Applicability and limitations in the characterization of poly-dispersed  
1539 engineered nanomaterials in cell media by dynamic light scattering  
1540 (DLS). *Mater*. 2019;12:3833.
- 1541 90. Gonzalez-Paredes A, Torres D, Alonso MJ. Polyarginine nanocapsules:  
1542 a versatile nanocarrier with potential in transmucosal drug delivery.  
1543 *Int J Pharm*. 2017;529:474-85.
- 1544 91. Ault AP, Stark DL, Axson JL, Keeney JN, Maynard AD, Bergin IL, et al.  
1545 Protein corona-induced modification of silver nanoparticle aggrega-  
1546 tion in simulated gastric fluid. *Environ Sci Nano*. 2016;3:1510-20.
- 1547 92. Walczak AP, Fokkink R, Peters R, Tromp P, Herrera Rivera ZE, Rietjens  
1548 IMCM, et al. Behaviour of silver nanoparticles and silver ions in an  
1549 in vitro human gastrointestinal digestion model. *Nanotoxicology*.  
1550 2013;7:1198-210.
- 1551 93. Coreas R, Cao X, Deloid GM, Demokritou P, Zhong W. Lipid and  
1552 protein corona of food-grade TiO<sub>2</sub> nanoparticles in simulated  
1553 gastrointestinal digestion. *Nanolmpact*. 2020;20:100272.
- 1554 94. Sakai-Kato K, Hidaka M, Un K, Kawanishi T, Okuda H. Physicochemical  
1555 properties and in vitro intestinal permeability properties and intes-  
1556 tinal cell toxicity of silica particles, performed in simulated gastrointes-  
1557 tinal fluids. *Biochim Biophys Acta*. 2014;1840:1171-80.
- 1558 95. Gelli R, Tempesti P, Ridi F, Baglioni P. Formation and properties of  
1559 amorphous magnesium-calcium phosphate particles in a simulated  
1560 intestinal fluid. *J Colloid Interface Sci*. 2019;546:130-8.
- 1561 96. Jiang X, Zhang X, Gray P, Zheng J, Croley TR, Fu PP, et al. Influences  
1562 of simulated gastrointestinal environment on physicochemical  
1563 properties of gold nanoparticles and their implications on intestinal  
1564 epithelial permeability. *J Environ Sci Heal Part C Environ Carcinog  
1565 Ecotoxicol Rev*. 2019;37:116-31.
- 1566 97. Gou J, Feng S, Liang Y, Fang G, Zhang H, Yin T, et al. Polyester-  
1567 solid lipid mixed nanoparticles with improved stability in gastro-  
1568 intestinal tract facilitated oral delivery of larotaxel. *Mol Pharm*.  
1569 2017;14:3750-61.
- 1570 98. Li Z, Ha J, Zou T, Gu L. Fabrication of coated bovine serum albumin  
1571 (BSA)-epigallocatechin gallate (EGCG) nanoparticles and their transport  
across monolayers of human intestinal epithelial Caco-2 cells. *Food  
Funct*. 2014;5:1278-85.
99. Ibrahim HM, Awad M, Al-Farraj AS, Al-Turki AM. Stability and dynamic  
aggregation of bare and stabilized zero-valent iron nanoparticles under  
variable solution chemistry. *Nanomaterials*. 2020;10:192.
100. Park S, Lee WJ, Park S, Choi D, Kim S, Park N. Reversibly pH-responsive  
gold nanoparticles and their applications for photothermal cancer  
therapy. *Sci Rep*. 2019;9:20180.
101. Asadi E, Azodi-Deilami S, Abdouss M, Khaghani S. Cyproterone syn-  
thesis, recognition and controlled release by molecularly imprinted  
nanoparticle. *Appl Biochem Biotechnol*. 2012;167:2076-87.
102. Jannin V, Deller E, Chevrier S, Chavant Y, Voutsinas C, Bonferoni  
C, et al. In vitro lipolysis tests on lipid nanoparticles: comparison  
between lipase/co-lipase and pancreatic extract. *Drug Dev Ind Pharm*.  
2015;41:1582-8.
103. Hosseinidou Z, Alam MN, Sim G, Tufenkji N, van de Ven TGM. Cellulose  
nanocrystals with tunable surface charge for nanomedicine. *Nanoscale*.  
2015;7:16647-57.
104. Wang J, Zhang L, Peng F, Shi X, Leong DT. Targeting endothelial cell  
junctions with negatively charged gold nanoparticles. *Chem Mater*.  
2018;30:3759-67.
105. Schleh C, Semmler-Behnke M, Lipka J, Wenk A, Hirn S, Schäffler M, et al.  
Size and surface charge of gold nanoparticles determine absorption  
across intestinal barriers and accumulation in secondary target organs  
after oral administration. *Nanotoxicology*. 2012;6:36-46.
106. Walczyk D, Bombelli FB, Monopoli MP, Lynch I, Dawson KA. What the  
cell "sees" in bionanoscience. *J Am Chem Soc*. 2010;132:5761-8.
107. Kumar S, Yadav I, Aswal VK, Kohlbrecher J. Structure and interaction of  
nanoparticle-protein complexes. *Langmuir*. 2018;34:5679-95.
108. Ranjan S, Dasgupta N, Sudandiradoss C, Ramalingam C, Kumar A. Tita-  
nium dioxide nanoparticle-protein interaction explained by docking  
approach. *Int J Nanomed*. 2018;13:47-50.
109. Bhogale A, Patel N, Sarpotdar P, Mariam J, Dongre PM, Miotello A, et al.  
Systematic investigation on the interaction of bovine serum albumin  
with ZnO nanoparticles using fluorescence spectroscopy. *Colloids Surf  
B Biointerfaces*. 2013;102:257-64.
110. Sasidharan A, Chandran P, Monteiro-Riviere NA. Biocorona bound gold  
nanoparticles augment their hemocompatibility irrespective of size  
or surface charge. *ACS Biomater Sci Eng*. 2016;2:1608-18.
111. Lundqvist M, Stigler J, Cedervall T, Berggård T, Flanagan MB, Lynch I,  
et al. The evolution of the protein corona around nanoparticles: a test  
study. *ACS Nano*. 2011;5:7503-9.
112. Maiorano G, Sabella S, Sorce B, Brunetti V, Malvindi MA, Cingolani R,  
et al. Effects of cell culture media on the dynamic formation of protein-  
nanoparticle complexes and influence on the cellular response. *ACS  
Nano*. 2010;4:7481-91.
113. Tsoi KM, MacParland SA, Ma X-Z, Spetzler VN, Echeverri J, Ouyang B,  
et al. Mechanism of hard-nanomaterial clearance by the liver. *Nat Mater*.  
2016;15:1212-21.
114. Yu M, Song W, Tian F, Dai Z, Zhu Q, Ahmad E, et al. Temperature- and  
rigidity-mediated rapid transport of lipid nanovesicles in hydrogels.  
*Proc Natl Acad Sci U S A*. 2019;116:5362-9.
115. Choki K, Li S, Ye A, Jameson GB, Singh H. Fate of hydroxyapatite nano-  
particles during dynamic in vitro gastrointestinal digestion: the impact  
of milk as a matrix. *Food Funct*. 2021;12:2760-71.
116. Levak M, Burić P, Dutour Sikirić M, Domazet Jurašin D, Mikac N, Bačić  
N, et al. Effect of protein corona on silver nanoparticle stabilization  
and ion release kinetics in artificial seawater. *Environ Sci Technol*.  
2017;51:1259-66.
117. Martin MN, Allen AJ, MacCuspie RI, Hackley VA. Dissolution, agglomerate  
morphology, and stability limits of protein-coated silver nanoparti-  
cles. *Langmuir*. 2014;30:11442-52.
118. Chao Y, Marsh AI, Behray M, Guan F, Engdahl A, Chao Y, et al. Synthesis  
and characterisation of isothiocyanate functionalised silicon nano-  
particles and their uptake in cultured colonic cells. *Faraday Discuss*.  
2020;222:332-49.
119. Marchiando AM, Graham WV, Turner JR. Epithelial barriers in homeosta-  
sis and disease. *Annu Rev Pathol*. 2010;5:119-44.
120. Van Spaendonck H, Ceuleers H, Witters L, Patteet E, Joossens J,  
Augustyns K, et al. Regulation of intestinal permeability: the role of  
proteases. *World J Gastroenterol*. 2017;23:2106-23.



- 1643  
1644  
1645  
1646  
1647  
1648  
1649  
1650  
1651  
1652  
1653  
1654  
1655  
1656  
1657  
1658  
1659  
1660  
1661  
1662  
1663  
1664  
1665  
1666  
1667  
1668  
1669  
1670  
1671  
1672  
1673  
1674  
1675  
1676  
1677  
1678  
1679  
1680  
1681  
1682  
1683  
1684  
1685  
1686  
1687  
1688  
1689  
1690  
1691  
1692  
1693  
1694  
1695  
1696  
1697
121. Brun E, Barreau F, Veronesi G, Fayard B, Sorieul S, Chanéac C, et al. Titanium dioxide nanoparticle impact and translocation through ex vivo, in vivo and in vitro gut epithelia. *Part Fibre Toxicol.* 2014;11:13.
  122. Cao X, Khare S, DeLoid GM, Gokulan K, Demokritou P. Co-exposure to boscalid and TiO<sub>2</sub> (E171) or SiO<sub>2</sub> (E551) downregulates cell junction gene expression in small intestinal epithelium cellular model and increases pesticide translocation. *Nanolmpact.* 2021;22:100306.
  123. Zhang Y, Duan S, Liu Y, Wang Y. The combined effect of food additive titanium dioxide and lipopolysaccharide on mouse intestinal barrier function after chronic exposure of titanium dioxide-contained feed-stuffs. *Part Fibre Toxicol.* 2021;18:8.
  124. Lee Y, Kamada N, Moon JJ. Oral nanomedicine for modulating immunity, intestinal barrier functions, and gut microbiome. *Adv Drug Deliv Rev.* 2021;179:114021.
  125. Tang M, Li S, Wei L, Hou Z, Qu J, Li L. Do engineered nanomaterials affect immune responses by interacting with gut microbiota? *Front Immunol.* 2021;12:684605.
  126. Goto Y. Epithelial cells as a transmitter of signals from commensal bacteria and host immune cells. *Front Immunol.* 2019;10:2057.
  127. Colombo G, Cortinovis C, Moschini E, Bellitto N, Perego MC, Albonico M, et al. Cytotoxic and proinflammatory responses induced by ZnO nanoparticles in in vitro intestinal barrier. *J Appl Toxicol.* 2019;39:1155–63.
  128. Busch M, Bredeck G, Kämpfer AAM, Schins RPF. Investigations of acute effects of polystyrene and polyvinyl chloride micro- and nanoplastics in an advanced in vitro triple culture model of the healthy and inflamed intestine. *Environ Res.* 2021;193: 110536.
  129. Kokalari I, Gassino R, Giovannozzi AM, Croin L, Gazzano E, Bergamaschi E, et al. Pro- and anti-oxidant properties of near-infrared (NIR) light responsive carbon nanoparticles. *Free Radic Biol Med.* 2019;134:165–76.
  130. Tyanova S, Temu T, Cox J. The MaxQuant computational platform for mass spectrometry-based shotgun proteomics. *Nat Protoc.* 2016;11:2301–19.
  131. Tyanova S, Temu T, Sinitcyn P, Carlson A, Hein MY, Geiger T, et al. The Perseus computational platform for comprehensive analysis of (prote) omics data. *Nat Methods.* 2016;13:731–40.
  132. Sambuy Y, De Angelis I, Rinaldi G, Scarino ML, Stammati A, Zucco F. The Caco-2 cell line as a model of the intestinal barrier: influence of cell and culture-related factors on Caco-2 cell functional characteristics. *Cell Biol Toxicol.* 2005;21:1–26.
  133. Dussert F, Wegner KD, Moriscot C, Gallet B, Jouneau P-H, Reiss P, et al. Evaluation of the dermal toxicity of InZnP quantum dots before and after accelerated weathering: toward a safer-by-design strategy. *Front Toxicol.* 2021;3:6.
  134. Konishi Y, Hagiwara K, Shimizu M. Transepithelial transport of fluorescein in Caco-2 cell monolayers and use of such transport in in vitro evaluation of phenolic acid availability. *Biosci Biotechnol Biochem.* 2002;66:2449–57.
  135. Balivada S, Rachakatla RS, Wang H, Samarakoon TN, Dani RK, Pyle M, et al. A/C magnetic hyperthermia of melanoma mediated by iron(0)/iron oxide core/shell magnetic nanoparticles: a mouse study. *BMC Cancer.* 2010;10:119.
  136. Jeitner TM. Optimized ferrozine-based assay for dissolved iron. *Anal Biochem.* 2014;454:36–7.
  137. ANalysis Of VAriance. p. [https://astatsa.com/OneWay\\_Anova\\_with\\_TukeyHSD/](https://astatsa.com/OneWay_Anova_with_TukeyHSD/).

## Publisher's Note

Springer Nature remains neutral with regard to jurisdictional claims in published maps and institutional affiliations.

1698  
1699  
1700

Ready to submit your research? Choose BMC and benefit from:

- fast, convenient online submission
- thorough peer review by experienced researchers in your field
- rapid publication on acceptance
- support for research data, including large and complex data types
- gold Open Access which fosters wider collaboration and increased citations
- maximum visibility for your research: over 100M website views per year

At BMC, research is always in progress.

Learn more [biomedcentral.com/submissions](https://biomedcentral.com/submissions)



Journal : **BMCTwo 12989**

Article No : **491**

MS Code :

Dispatch : **7-7-2022**

LE

CP

Pages : **28**

TYPESET

DISK

Journal:	<b>12989</b>
Article:	<b>491</b>

## Author Query Form

**Please ensure you fill out your response to the queries raised below and return this form along with your corrections**

Dear Author

During the process of typesetting your article, the following queries have arisen. Please check your typeset proof carefully against the queries listed below and mark the necessary changes either directly on the proof/online grid or in the 'Author's response' area provided below

Query	Details Required	Author's Response
<a href="#">AQ1</a>	Affiliations: Please check and confirm that the authors and their respective affiliations have been correctly identified and amend if necessary.	
<a href="#">AQ2</a>	Article structure: Please confirm the section headings are correctly identified.	
<a href="#">AQ3</a>	Table: Please provide a definition for the significance of italics values in the Table 4.	
<a href="#">AQ4</a>	Additional file: As per journal requirements, every additional file must have a corresponding caption; however, no caption is provided inside the manuscript. Please supply the missing caption of Additional file 1.	